

DAOSPEC: an automatic code for measuring equivalent widths in high-resolution stellar spectra

Peter B. Stetson¹

*Herzberg Institute of Astrophysics, National Research Council of Canada, 5071 West Saanich Road,
Victoria, BC V9E 2E7, Canada*

`Peter.Stetson@nrc-cnrc.gc.ca`

and

Elena Pancino

INAF – Bologna Observatory, via Ranzani 1, I-40127 Bologna, Italy

`elena.pancino@oabo.inaf.it`

ABSTRACT

DAOSPEC is a Fortran code for measuring equivalent widths of absorption lines in stellar spectra with minimal human involvement. It works with standard FITS format files and it is designed for use with high resolution ($R > 15000$) and high signal-to-noise-ratio ($S/N > 30$) spectra that have been binned on a linear wavelength scale. First, we review the analysis procedures that are usually employed in the literature. Next, we discuss the principles underlying DAOSPEC and point out similarities and differences with respect to conventional measurement techniques. Then experiments with artificial and real spectra are discussed to illustrate the capabilities and limitations of DAOSPEC, with special attention given to the issues of continuum placement; radial velocities; and the effects of strong lines and line crowding. Finally, quantitative comparisons with other codes and with results from the literature are also presented.

Subject headings: Data Analysis and Techniques

1. Introduction

Most of the information we acquire about the chemical compositions and atmospheric parameters of stars comes from spectral absorption features, both molecular bands and atomic lines. One of the most powerful and well-understood techniques to disentangle the chemical abundance from, for instance, the effects of temperature and gravity on absorption features employs measurements of equivalent widths (EWs).

Usually, chemical abundances are best derived when the EW analysis is based upon high-resolution ($R = \lambda/\delta\lambda \gtrsim 15000$) spectra with relatively high values of the signal-to-noise ratio ($S/N \gtrsim 30$). This level of data quality was typical of the best that could be achieved in the 1970s and now it has become a sort of lower limit for the standard² quality expected for deriving accurate chemical abundances from optical spectra ($\lambda \sim 3200 - 10000 \text{ \AA}$). Recently, it has become possible to achieve similar data quality ($R \simeq 10000$, $S/N \simeq 30$) in the near infrared wavelength range (up to K -band wavelengths, $\lambda \simeq 2.2 \mu\text{m}$).

As technology has advanced rapidly in the last

¹Based on data obtained from UVES@VLT, GIRAFFE@VLT, HARPS@VLT located in the ESO observatory of Cerro Paranal, Chile. Also based on data from FOCES@CAHA 2.2m telescope in Calar Alto, Spain. Data from the VALD and GEISA online databases has been employed as well.

²Typically, $R \simeq 40000$ and $S/N \simeq 50-100$ are used in the optical.

few decades, telescopes of increasingly larger aperture have become available, as well as spectrographs that allow us not only to reach very good resolution and flux fidelity, but also to observe many objects simultaneously. It has now become commonplace to work on sets of hundreds of high-resolution spectra from fiber spectrographs such as, e.g., FLAMES mounted at the European Southern Observatory Very Large Telescope in Chile (Pasquini et al. 2002). Our knowledge of atomic constants for many of the absorption lines present in stellar atmospheres has also advanced and we are now typically able to use several tens of lines for a few dozens of different chemical species.

The actual process of measuring EWs has until recent years mostly been tackled with the help of interactive graphical software, such as IRAF³ or MIDAS (Warmels 1992). However, this procedure has two main drawbacks: *(i)* lines are usually identified by the user in a non-automatic way, and the measurement of each individual line requires—to say the least—several seconds of direct human involvement (lack of *performance*); *(ii)* a certain degree of subjectivity is involved in the measurement process, particularly due to the continuum placement by the user around each line; this means that different users could produce different results from the same data (lack of *robustness*). It may also be noted that the tedium of the process itself often discourages a thorough testing of the procedures via repeated measuring under different sets of assumptions and protocols.

Therefore, given the vastly increased volume of data and the better data quality available these days, the community has started writing (semi-)automatic codes that improve both the performance of the measuring process and the robustness of the results. Most of these codes are not really public, in the sense that they are designed to meet the specific goals of some research group and are provided on a personal basis to close collaborators.

DAOSPEC is a Fortran code to measure EWs of atmospheric absorption lines in high resolution spectra. Our goal is to provide the performance

required by the increasing amount of data available; the convenience and repeatability of a fully automatic routine; and availability to the whole astronomical community. With the help of simple shell scripts, detailed in the DAOSPEC Cookbook (Pancino & Stetson 2008), a large number of stars with different characteristics and configurations can be processed in a fully automatic and unsupervised way. Effort has been put into making the code compatible with standard astronomical image formats such as the FITS standard (Wells et al. 1981; Calabretta & Greisen 2002; Greisen & Calabretta 2002; Greisen et al. 2006) and to use standard Fortran coding and libraries.

One advantage of a fully automatic code that is also publicly available is that the results are reproducible and testable in variety of conditions of use and by many different users. Indeed, such a set of independent tests is presently under way in the small but growing community of DAOSPEC users (see also Section 4).

In Section 2 below we describe the EW measurement process in general, and its implementation in a few public software packages; in Section 3 we give a general description of DAOSPEC itself; in the various subsections, we discuss in depth a few topics which are relevant to the most common scientific cases, including radial-velocity determination (Section 3.1); continuum placement (Section 3.2); strong lines and blended lines (Section 3.3); uncertainty estimates (Section 3.4); and dependence of the results on the choice of input parameters (Section 3.5) and on spectral quality (Section 3.6). Some performance considerations are also presented (Section 3.7). Comparisons with other codes and with previously published measurements are presented and discussed in Section 4. Finally, in Section 5 we summarize our conclusions.

2. EW Measurements in General

Figure 1 illustrates how the EW of a spectral line is defined, starting from the continuum level (I_C) and the specific flux at the line center (I_0). The EW represents the strength of an absorption line, and it is defined as the width, in wavelength units, that a rectangular stripe of height I_C , in intensity units, would have if it had the same area as the actual line or—in other words—the wave-

³Image Reduction and Analysis Facility. IRAF is distributed by the National Optical Astronomy Observatories, which is operated by the association of Universities for Research in Astronomy, Inc., under contract with the National Science Foundation

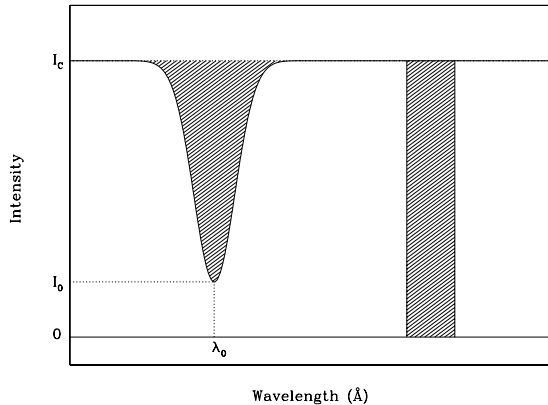


Fig. 1.— Classical definition of EW: the width of a rectangular line (right) with the same area as the actual absorption line (left). See text for details. I_c is the continuum level while I_0 is the specific flux at the line center λ_0 , measured upward from zero.

length interval that would be covered by a hypothetical, perfectly opaque absorption feature that removes the same amount of energy from the continuum flux. More practically, for an isolated spectral line in a discretely-sampled spectrum from a real instrument:

$$EW = \Delta\lambda \sum_i \frac{I_{C_i} - I_i}{I_{C_i}} \quad (1)$$

where $\Delta\lambda$ is the (constant) pixel size, I_{C_i} is the continuum level at the wavelength of the i -th pixel, and I_i is the actual flux received by the i -th pixel.

In a real spectrum, however, noise, spectral defects and neighboring lines can affect the perceived profile of an absorption line, and an EW is not necessarily readily measured as a direct summation of the pixel fluxes. Since the line profile is generally dominated by the point-spread function of the slit image, which can often be approximated by a Gaussian profile⁴ (see Section 3.3), often a *numerical fit* of a Gaussian-shaped function $g(\lambda)$ is adopted instead of the direct numerical summation:

$$g(\lambda) = A e^{-(\lambda - \lambda_0)^2 / 2\sigma^2}, A > 0 \quad (2)$$

⁴Different line profiles (i.e., Voigt, Lorentz) can be adopted for lines that significantly deviate from the Gaussian form.

$$I_i = I_{C_i} [1 - g(\lambda_i)] \quad (3)$$

(i.e., the specific flux I_i assumes a minimum value $I_0 = I_{C_i} - A$ at $\lambda_i = \lambda_0$, and $I_i \rightarrow I_{C_i}$ for λ_i far from λ_0). The estimated EW thus becomes

$$EW = \sum_i \frac{I_{C_i} - I_i}{I_{C_i}} \Delta\lambda \rightarrow \int g(\lambda) \lambda \quad (4)$$

where $\Delta\lambda$ is the step of the integration process that can be made very small ($\rightarrow d\lambda$).

No measurement means much without an associated uncertainty. When fitting lines to obtain EWs with Equation 4 in a digital computer, a standard error can be computed for each line with various mathematical techniques that estimate the goodness of the fit (e.g., least-squares formal errors). These confidence intervals can also take into account the quality of the spectrum (R, S/N, and—to a certain extent—crowding and spectral defects, etc.). Cayrel (1988) gives approximate formulae for estimating the uncertainty of an EW as a function of spectral quality:

$$\delta EW \simeq 1.5 \frac{\sqrt{\Delta\lambda \cdot FWHM}}{S/N} \simeq 1.6 \frac{\sqrt{\Delta\lambda \cdot EW}}{S/N} \quad (5)$$

where FWHM is the the full width at half maximum of the line. (For a perfect Gaussian profile, $FWHM = 2.355 \sigma$.) Of course, as noted in the paper by Cayrel (1988), this is a lower limit to the actual uncertainty because the true continuum level is never perfectly known, but it too has an associated uncertainty that should be propagated through the whole calculation. However, the effect of continuum placement (see below) is very difficult to take completely into account.

Ways to estimate the uncertainty due to the continuum placement in each pixel have been obtained by Ramírez et al. (2001), Bohlin et al. (1983) and Levshakov et al. (2002) among others. The idea is that the derivative of Equation 4 has to be computed not only with respect to I_i but also with respect to the continuum level in each pixel, I_{C_i} , and the total uncertainty then becomes⁵

⁵For those programs that evaluate the continuum *locally* in two windows beside each line, the full uncertainty can also be estimated with the alternate method provided by Bohlin et al. (1983).

$$\delta EW = \sqrt{\left(\sum_i (\delta I_i)^2 \frac{\partial EW}{\partial I_i}\right)^2 + \left(\sum_i (\delta I_{C_i})^2 \frac{\partial EW}{\partial I_{C_i}}\right)^2} \quad (6)$$

where δI_i and δI_{C_i} are the uncertainties on I_i and I_{C_i} , respectively; e.g. these would be the Poisson errors $\sqrt{I_i}$ and $\sqrt{I_{C_i}}$ if the spectra are in units of raw detected photoelectrons. Otherwise, of course, the errors must be appropriately adjusted for any renormalizing of the data. As pointed out by Levshakov et al. (2002), the above formula still provides only an estimate of δEW because when the spectra are resampled to constant wavelength bins, the errors in the single pixels become correlated. The correlation term that should be added to Equation 6 appears to be small, and as we will see in Section 3.2, there are other uncertainty sources that dominate the continuum error budget, such as line crowding and blanketing by very weak lines.

A very simple experiment shows the impact of continuum placement on the EW measurements. An observed spectrum of star 2129 in the open cluster Collinder 110 (Pancino et al., in preparation) was normalized to an arbitrary “best” continuum in the range 5500–6500 Å and the EW of ~ 50 lines were measured with the task *splot* in IRAF. This spectrum has a resolution of $R \simeq 30000$ and a S/N ratio of approximately 75 (per pixel). Later, the lines’ EWs were remeasured adopting a continuum level higher or lower than the adopted “best” continuum by 1%, 3%, 5% and 10%, respectively. The resulting ΔEW values are shown in the four panels of Figure 2. As can be seen, except for a few lines with the smallest EWs, all measured line strengths are altered by approximately constant values: $\sim \pm 3$ – 3.5 mÅ in the case of a $\pm 1\%$ misplacement, $\sim \pm 9.5$ mÅ in the $\pm 3\%$ case, $\sim \pm 16$ mÅ in the $\pm 5\%$ case, and $\sim \pm 30$ – 32 mÅ in the pessimistic case of a 10% misplacement. Of course, noise, resolution, line crowding and line blanketing also have an impact on the actual ΔEW values, but the above experiment gives a quantitative idea of what happens when the continuum level is badly misestimated (see also Section 3.4.3).

In the following subsections we examine the various operational steps that must be undertaken

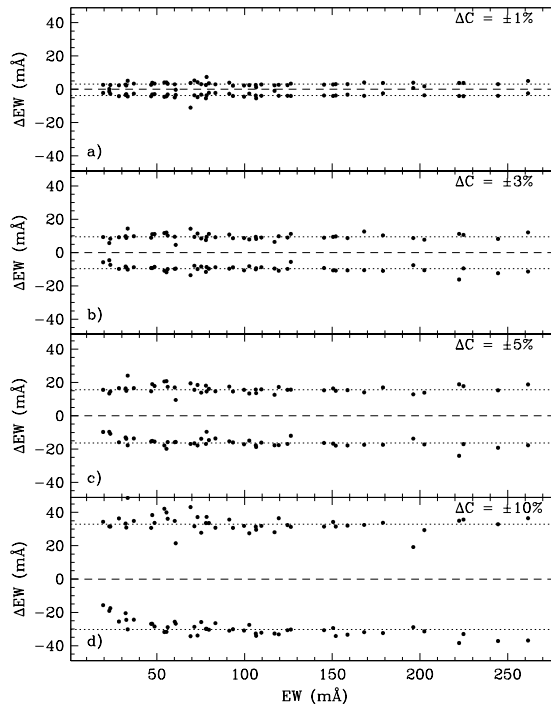


Fig. 2.— Differences between EW measured on the adopted “best” continuum level and the EW of the same lines measured on a continuum level altered by $\pm 1\%$ (Panel a), $\pm 3\%$ (Panel b), $\pm 5\%$ (panel c) and $\pm 10\%$ (Panel d). The spectrum is that of star 2129 in the open cluster Cr 110 (Pancino et al., in preparation)

when measuring the EW of a line. We will provide practical examples based on a few publicly available programs. The IRAF task *noao.oned.splot* is taken as a good representation of those graphical interactive packages that allow the user to manually⁶ measure EWs from their spectra; we believe that inferences drawn from the IRAF package will apply to other analogous routines, such as that provided within MIDAS, and others. The Fortran program SPECTRE⁷ (Fitzpatrick & Snenen 1987) is taken as an example of a more automated routine and since it is part of the widely

⁶When dealing with many spectra having similar characteristics, many users develop their own pipelines in the IRAF script language or the MIDAS equivalent, but these pipelines cannot really be considered here, since they are often highly specific to the problem treated and are seldom made public.

⁷<http://verdi.as.utexas.edu/spectre.html>

used MOOG package⁸ (Snedden 1973) it serves as a very good reference in the following discussion. ARES (Sousa et al. 2007) and EWDET (Ramírez et al. 2001) are two programs written in C++ and Fortran respectively. Although not entirely objective (due to user involvement in the continuum placement, see Section 2.2), to our knowledge they are the only fully automated codes publicly available⁹.

2.1. Line Finding and Identification

Within interactive tasks such as *splot* or SPECTRE, the processes of line *finding* and *identification* are generally joint and happen in the same initial phase of the measurement. By *line finding* we mean the process of specifying where in the observed spectrum are perceived dips representing good candidate absorption lines. By *line identification*, on the other hand, we mean the process of specifying which of the perceived absorption features corresponds to a particular atomic transition. The latter task requires some knowledge of the radial velocity of the star to infer the rest wavelength of the line for comparison with laboratory line lists.

Within IRAF, *splot* requires the user to mark with the cursor, on a radial-velocity-corrected spectrum, the continuum position on both sides of a line. Apart from helping to define the continuum level, this also tells the program the line’s approximate location (*initial finding*). The program then fits the appropriate function and determines a precise wavelength for the line center (*refined finding*), as well as the EW. Finally the user confirms whether the measured line center is acceptably close to the laboratory wavelength (*identification*).

SPECTRE also needs a radial-velocity-corrected spectrum as input, and accepts entry of the laboratory wavelength of a line (or reads a list of wavelengths from a file). The measuring process *per se* has a similar structure to that of IRAF: *initial finding* based upon the rest wavelength,

refined finding (and fitting) of the perceived absorption feature closest to the rest wavelength and final *identification* by decision of the user. In the easiest cases, users just need to provide SPECTRE with the spectrum and a line list, and to check subsequently whether the program has done a good job. Thus, the procedure can be much faster than with IRAF. However, SPECTRE also provides several interactive tools to improve the fit in more difficult cases, such as continuum adjustments, the use of partial line profiles, and others.

In ARES and EWDET, *line finding* is completely automatic and independent from the *identification* procedure.

ARES uses local maxima of the second derivative—defined as zeros of the third derivative—to identify the centers of absorption lines. In the paper that presents the code, Sousa et al. (2007) have shown (see, e.g., their Fig. 3; see also Section 2.3 below) that this approach can enhance the detection of highly blended lines not readily apparent in the original spectrum. However, the effect of noise dramatically propagates in the numerical derivatives even for spectra with high S/N ratios. Therefore, in practice the observed spectrum is artificially smoothed to reduce confusion between noise and real features before computing the numerical derivatives. This is especially important since the FWHM is left as a free parameter (see Section 2.3) and cannot therefore be used to distinguish between an absorption line and a noise artifact. To avoid further problems, the input parameter *lineresol* tells the code the minimum distance between lines in Ångströms. ARES requires that the spectrum be pre-corrected for the radial velocity to identify detected lines with entries in the input line list on the basis of their rest wavelengths.

In EWDET, the spectrum is examined, pixel by pixel, to find all the points that deviate from a previously found continuum by more than 2σ . Those points are further examined to see whether they have neighbors that also deviate from the continuum, and if so, the line *finding* is considered complete. The *line identification* is left to the user in the case of EWDET, and, to facilitate this task, the radial velocity is used as an input to compute the rest wavelength of each line.

One side effect of all these methods, which can considerably slow down the procedure, is that the

⁸<http://verdi.as.utexas.edu/moog.html>

⁹We are aware of the existence of other codes that are not really public, and therefore are not considered in the following discussion. For instance, one such program, ROSA, has been written by R. Gratton (E. Carretta, private communication) and another, *fitline*, by P. François (P. François, private communication).

radial velocity of each star must be known *a priori*. In some cases, as we have seen, the input spectrum must already be shifted to zero radial velocity.

2.2. Continuum Placement

Continuum placement is a source of uncertainty for any EW measurement, and there is as yet no generally accepted best practice in estimating the continuum level in a stellar spectrum densely populated with absorption lines. For instance, when writing a program for extracting EWs, one must consider whether to use a *local* or *global* continuum normalization, or a combination of the two. The approach employed in DAOSPEC will be examined in depth in Sections 3 and 3.2. Here, we describe the procedures adopted by SPECTRE, *splot*, ARES and EWDET.

SPECTRE requires spectra that are already roughly normalized to their continua. This is necessary because the user can only, if needed, readjust the local continuum *level* and not its global *shape*. Therefore it is optimal to normalize spectra that have steep or strongly curved continua before feeding them to SPECTRE.

IRAF/*splot* allows the user to mark separate left and right continuum levels relative to the chosen line, and these can have very different values. However, since the continuum level *within* the absorption line is evaluated by interpolating a straight line between the two continuum samples, a preliminary continuum correction is again desirable in the case of strongly curved or steep spectra. At least one of the private packages of which we are aware (E. Carretta, private communication) also chooses to normalize the continuum based on windows on the short- and long-wavelength sides of each absorption line. So, this package, like both SPECTRE¹⁰ and *splot*, therefore requires (or gives better results after) a *global* continuum normalization, i.e., the procedure of dividing the whole spectrum by a fitting function (usually a polynomial or a spline function), followed by minor *localized* continuum adjustments.

ARES also finds the continuum level locally around each line, using a $\kappa\sigma$ rejection algorithm. The parameters of the fit and of the $\kappa\sigma$ rejection,

however, are highly customizable and flexible. This is the only point in ARES where the user has a strong impact on the outcome: trying many different combinations of parameters is important for guaranteeing a good result, and an inexperienced user can obtain worse results than an experienced or extremely careful user, as can also happen with *noao.oned.continuum*. Moreover, the best combination of parameters will change for different sets of spectra, and various users will have different opinions on how the continuum should be placed. In summary, continuum placement is the main reason why the results obtained with ARES cannot be considered entirely objective.

EWDET chooses a *global* continuum normalization approach: the continuum determination is done by automatically fitting a curve to the whole spectrum with several iterations of point rejection above and below sigma levels specified by the user. This is not significantly different from what is done in the IRAF task *noao.oned.continuum*, and as in the case of ARES, it introduces a certain degree of subjectivity in the process. EWDET however, unlike other programs, stores in its memory the uncertainty of the continuum placement and uses it in the computation of the final EW uncertainty (see Section 2.4).

The choice of the continuum normalization method is crucial and will be discussed further in Section 3.2.

2.3. Line Fitting

IRAF offers the widest range of possibilities: a line can be measured by summation of the pixel values (i.e., without any fitting procedure, Equation 1), or by fitting a Gaussian function (Equation 4), a Voigt profile, or a Lorentz profile. The task can measure both absorption and emission lines. Finally a deblending routine is also available, where the user interactively marks the region to investigate, the peaks of the blended lines, and so on. SPECTRE offers similar options, although it is more specifically designed for the classical analysis of isolated absorption lines. ARES and EWDET use Gaussian profiles, performing fits similar to our Equation 4 and reporting the fit parameters in their output files. ARES, however, appears to be able to fit a line with multiple Gaussian functions to improve the fit of each line profile, and the number of Gaussians actually used

¹⁰We point out that SPECTRE provides additional tools that help continuum fitting, such as the one colloquially known as *boinking*.

is listed in the output file.

Thus, the most widely used profile is a Gaussian function. Generally speaking, three parameters are free in the fit: the centroid λ_0 , the standard deviation σ or, equivalently, the full-width at half-maximum, and the depth of the line center (A in the notation of our Equation 4). Of these three, here we consider the FWHM. In an observed spectrum, the line profile is a convolution of the instrumental profile with an intrinsic line profile. At the resolution that is typically used for routine abundance analysis (i.e., from $R \sim 20,000$ to $R \sim 50,000$), the line profile is still dominated, for most lines, by the instrumental profile, which either is the same for all lines, or scales as the wavelength when multiple echelle orders are patched together. Therefore, in principle, there is no need to leave this parameter free for each individual line once the instrumental characteristics have been determined.

Most existing packages, however, choose to leave this parameter free for each line, as is done in *splot*, SPECTRE, ARES, and EWDET. As an advantage, the derived FWHM can be used *a posteriori* to indicate whether a line has been properly measured: lines with a FWHM significantly larger than average are most probably unresolved blends, while lines with a FWHM significantly smaller than average could be noise spikes, telluric features, or spectral defects. Another positive side of this approach is that it compensates, to some degree, for saturation. When a line becomes strong enough to just enter the saturation regime, it can still be mimicked with a slightly wider Gaussian, with a modest error in the EW measurement (of course, very strong lines cannot be correctly reproduced this way.) The main disadvantage is allowing the FWHM to be completely free complicates the deblending capabilities of an automated program when the noise level in the spectrum is appreciable. Most obviously, an apparently broad feature could be modeled by a single profile with a large FWHM or by multiple narrower profiles. Moreover, even when the number of components in a blend is considered known, numerical degeneracies between the widths and strengths of the various overlapping features increase the uncertainties in the fitting parameters that are produced by the analysis.

2.4. Uncertainty Evaluation

Uncertainties in the measurement of EWs are often neglected when deriving chemical abundances. Often, having measurements of n lines for some chemical element, it is convenient to compute the mean and variance of the single-line abundances and to use $\sigma/\sqrt{n-1}$ as the uncertainty of the net abundance adopted for that particular element. Using a good estimate of the EW uncertainty of each line to perform a weighted average would give somewhat better results, but the dominant source of uncertainty in the adopted chemical abundances is often the uncertainty in the stellar atmospheric parameters. This explains at least in part why little effort is sometimes put into evaluating EW uncertainties (see also Section 2).

Still, when writing a package that measures EWs, individual uncertainties can easily be estimated, and indeed they are of fundamental importance in particular cases, e.g., temporal variations of the EW. In the case of *splot*, each of the pixels used in the fit is assigned its own standard error through the construction of a statistical noise model based on Poisson photon noise (read-out noise is usually negligible for spectra with high S/N ratios). The error estimate, however, is optional and can only work if the user inputs an appropriate gain value if the spectral intensities are recorded in some instrumental data-number units rather than in raw detected photoelectrons. Furthermore, if the input spectrum has been prenormalized with a flat-field spectrum or to a provisional continuum, the numerical conversion from Poisson errors to intensity-unit errors will be a function of wavelength. In SPECTRE and ARES, no error computation routine is provided, for the reasons outlined above. EWDET, on the other hand, performs a full error computation that is described in detail by Ramírez et al. (2001). In short, each pixel used in the fit is assigned its own uncertainty estimate based on propagation of errors through the Gaussian fitting procedure¹¹, including the continuum placement uncertainty, which is almost never considered in other packages. Pixel

¹¹The Gaussian fit used by Ramírez et al. (2001) is different from our Equation 4, in that the formula by Ramírez et al. (2001) is strictly valid only when $I_C=1$, while our formula is valid in the general case, even if $I_C \neq 1$.

uncertainties are then summed in quadrature after multiplication by the pixel size.

3. DAOSPEC

DAOSPEC¹² is a code written in standard Fortran 77. The version that we have made generally available makes use of the cfitsio libraries¹³ (Pence 1999) for dealing with standard FITS-format spectra. IRAF format (.imh, .pix) files can also be used, and we have included an optional graphical display¹⁴ that allows the user to monitor the progress of the analysis. However, none of these should be considered an integral or essential part of the algorithms we discuss here. Practical and detailed help on how to obtain, install, and use DAOSPEC can be found in the DAOSPEC Cookbook¹⁵ (Pancino & Stetson 2008), or by directly contacting the authors.

We briefly describe here the general code structure depicted as a flow chart in Figure 3. More details on the most important steps are given in the following subsections. The reduction path consists of three main stages: (i) the input and preparation phase, shown on the left side of Figure 3; (ii) the main iteration loop, center of Figure 3 and (iii) the evaluation and output phase, right side of Figure 3.

Three inputs, shown on the left side of Figure 3, are needed: (i) a small set of configuration parameters, specifying among other things the wavelength limits of the spectral region of interest, a first guess at the FWHM, the order of the polynomial to be used for the continuum normalization, and other basic information required by the code; (ii) the reference line list, which contains the laboratory wavelengths of as many clean and unblended lines as possible, and may contain any additional textual information—such as atomic parameters and notes—that the user finds convenient; and (iii) a spectrum in standard FITS or IRAF format, which must be binned linearly with wavelength. Items (i) and (ii) are specified once at the very beginning of the reduction pro-

cess; any number of individual spectra (iii) may be then analysed one after another, at the user’s pleasure. A more detailed description of this procedure is given in the Cookbook.

With the above inputs, the code performs an initial continuum fit with the help of Legendre polynomials of the order specified by the user, and performs the line finding procedure (see also Section 3.1). Then, a preliminary correlation of detected lines with the input list of laboratory wavelengths is performed, to derive an initial radial-velocity estimate.

Now the main loop starts (center of Figure 3). The detected lines are provisionally subtracted from the spectrum and the remaining residual spectrum is used to refine the continuum normalization (see also Section 3.2) by means of robust non-linear least squares. With the newly normalized spectrum, the individual line centroids and strengths are then refined, along with a value for the FWHM which is either constant for all lines, or considered to be a linear function of wavelength (see also Section 3.3). This whole procedure is repeated five times. (The number “five” was chosen arbitrarily and—so far—it appears to be adequate. It can be changed trivially if future experience indicates a need.)

After final execution of the refinement loop, the fitted wavelengths of the individual lines are compared to the table of laboratory wavelengths. A simple outlier-clipping algorithm is used to determine the final radial-velocity estimate for the star and, at the same time, to specify which of the detected lines lie sufficiently close to tabulated laboratory wavelengths to be regarded as legitimate detections of particular atomic transitions. Equivalent widths are computed from the fitted line parameters, and uncertainties in those EWs are determined from the residual noise remaining in the spectrum within the wavelength range of the line profile (see also Section 3.3).

The code output is a text file containing in its header the estimated FWHM at the center of the spectrum; the estimated radial velocity of the star with its standard error; the number of lines used to determine the velocity; and the root-mean-square value of the pixel-by-pixel flux residuals remaining in the spectrum after subtraction of all the fitted lines, expressed as a percentage of the fitted continuum flux. Following that, the file contains

¹²<http://cadwww.dao.nrc.ca/stetson/daospec/>
<http://www.bo.astro.it/~pancino/projects/daospec.html>

¹³<http://heasarc.nasa.gov/docs/software/fitsio/fitsio.html>

¹⁴“SuperMango:” <http://www.astro.princeton.edu/~rhl/sm/>

¹⁵<http://cadwww.dao.nrc.ca/stetson/daospec/daospec.ps>
<http://www.bo.astro.it/~pancino/docs/daospec.pdf>

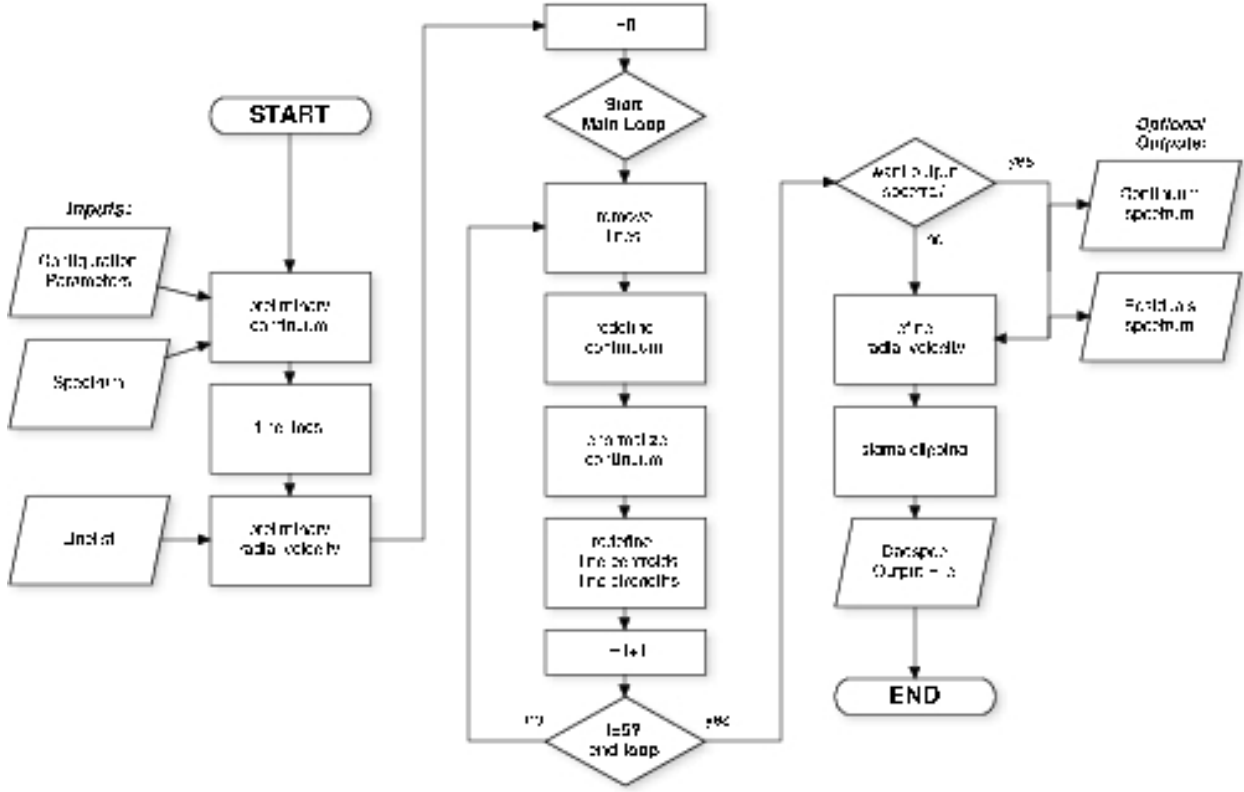


Fig. 3.— Flow chart diagram for DAOSPEC.

a list of all the lines found by DAOSPEC having strengths greater than a user-specified minimum EW. Both their observed and inferred rest wavelengths are reported, these latter computed on the basis of the estimated radial velocity. If a particular detected line has been identified with an entry in the input line list, the laboratory wavelength of the line along with any additional textual information from the input line list is also reproduced in the output.

Optionally, (right side of Figure 3), the code can be instructed to produce two FITS- or IRAF-format spectra, one containing the final estimated polynomial continuum model used to normalize the spectrum, and another containing the spectrum of the flux residuals, of the flux residuals, after the spectrum has been divided by the fitted continuum and all the lines found by DAOSPEC have been fitted and digitally subtracted.

3.1. Line finding, line identification and radial velocity

Line finding in DAOSPEC is performed with the help of a tuned second-derivative filter to identify local minima. The user-specified initial guess of the FWHM is used to optimize the distinction between valid lines and noise or continuum features¹⁶. During the main iteration loop (see Figure 3) the initial FWHM estimate is refined at the same time as the line centroids and strengths, by the method of robust non-linear least squares, and provisional line detections are abandoned if refined EW estimates indicate they are too weak to be of interest. Note that, as mentioned above, the user may specify whether the FWHM is to be regarded as constant over the entire wavelength range of the spectrum, or as proportional to wavelength.

Preliminary line identification is performed by

¹⁶This means that DAOSPEC is effective in separating noise from real spectral features as long as the FWHM of a line is adequately sampled, i.e., by at least 2 pixels.

a simple cross-correlation of the detected lines with the input list of laboratory wavelengths: that wavelength shift that corresponds to the greatest number of matching lines is adopted as indicating the preliminary radial-velocity estimate for the star. (The user can help make this process reliable by supplying as *complete* and *appropriate* a line list as possible for the anticipated spectral class of the star, and for the presumably known wavelength range, resolution, and S/N ratio of the spectra.) After completion of the main refinement loop, these cross-identifications are reconsidered on a line-by-line basis. A particular cross-identification of a detected line with a laboratory transition is regarded as valid if the radial velocity implied by that provisional identification agrees with the adopted final radial velocity of the star within a user-specified tolerance. Therefore, once the laboratory line list and the significance and identification tolerances have been specified by the user, both the line *finding* and *identification* procedures are completely automated, and the observed radial velocity of the star is one of the program *outputs*, not *inputs*. This has an impact on performance, as discussed in Section 2.1.

The final radial-velocity measurement is provided together with its line-by-line variance, (σ), and the number of lines (n) actually used in its determination. These can in principle be combined to provide a final error estimate as $\sigma/\sqrt{n-1}$. However, when measuring spectra that have not been specifically intended for high-precision radial-velocity measurements, special care must be taken. For example, if there are thermal changes between daytime lamp observations and night-time star observations, or if the star image can be off-center in a finitely wide spectrograph slit, there may well be systematic velocity errors that are not reflected in the line-by-line velocity variance.

There is the possibility of correcting for these effects if at least one of the telluric absorption bands¹⁷ of O₂ or H₂O is included in the observed spectral range. A very accurate list of rest wavelengths of atmospheric absorption lines can be

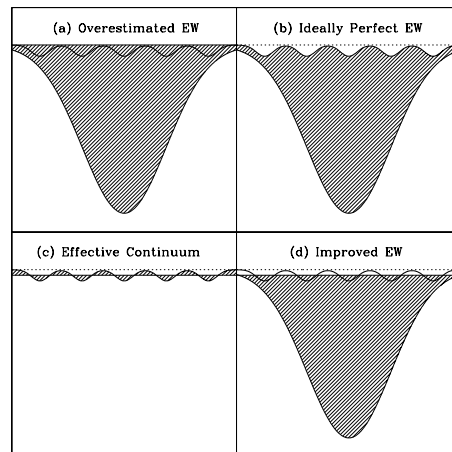


Fig. 4.— Effect of different choices of the continuum (see text for details). Panel (a): A strong spectral line is sketched as a Gaussian; small lines and spectral defects (small Gaussians) pollute the line; if the EW is measured with respect to the *true continuum* (horizontal line), it will be overestimated because the flux absorbed in the weak lines will be added to the flux absorbed in the strong line. Panel (b): as before, but now the shaded area represents the true amount of flux absorbed in the strong line alone, exclusive of the flux removed from the spectrum by the weak lines. Panel (c): here the strong spectral line has been fitted and removed, and the *effective continuum* (solid line) is obtained by balancing to zero the residuals (dashed area), which include noise (not represented here for clarity) and all the small polluting features (small Gaussians); the *effective continuum* (dotted line) is therefore lower than the *true continuum*. Panel (d): the EW is now estimated with respect to the *effective continuum*, a depressed continuum that includes, statistically, the effect of typical local pollution by weak lines; the EW estimate is thus improved.

obtained from the GEISA¹⁸ database (Jacquinet-Husson et al. 1999, 2005). A separate measurement can be performed using such a telluric line

¹⁷We remind the reader that while night-sky *emission* lines can be used to identify and correct thermal or other changes in spectrograph alignment, they *cannot* be used for correcting errors due to mis-centering of the star in the slit since the sky illuminates the slit uniformly.

¹⁸Gestion et Etude des Informations Spectroscopiques Atmosphériques, <http://ara.lmd.polytechnique.fr/htdocs-public/products/GEISA/HTML-GEISA/>

list as input and forcing DAOSPEC to explore a limited radial velocity range close to 0 km s^{-1} . Our experience on red giants in ω Centauri¹⁹ (Pancino et al. 2007) and in open clusters²⁰ (Pancino et al., in preparation) shows that the radial velocity shifts measured in the telluric absorption lines can be up to $1\text{--}3 \text{ km s}^{-1}$ and, what is more important, the associated uncertainty can be of order 0.5 km s^{-1} . However, when these measurements are used as *corrections* to the stellar radial velocities, formal errors of $0.1\text{--}0.3 \text{ km s}^{-1}$ can be easily achieved.

3.2. Continuum Normalization

What is generally understood as the *continuum* of a spectrum is the level of flux that one would have if *only* continuum-opacity sources—i.e., no discrete absorption lines or bands—were present: we will call this the *true continuum*. Traditionally we seek the true continuum to anchor our fitting function when measuring the EW of a particular line (Equations 1 and 4). This is appropriate when the spectra are not crowded and the line in question is not contaminated by neighboring lines. Otherwise, true continuum determinations are particularly difficult and in most cases it is also very difficult to state the associated uncertainty. Moreover, we contend that when measuring lines in crowded spectra, what we really want to determine is *not* the true continuum level at all.

In fact, we are trying to estimate how much flux one particular atomic transition is subtracting from the net output flux of the stellar atmosphere. But we need to separate that from the flux subtracted (or added) by other contaminating effects, such as: (i) other atomic or molecular lines that are too weak or too close to our line to be distinguished; (ii) the noise, which for an infinite number of pixels should give an average zero contribution, but for a small number of pixels could give a non-zero contribution; (iii) detector defects; and (iv) artifacts from the imperfect removal of cosmic rays, sky emission lines and telluric absorption features. Therefore, even if we

¹⁹Using ESO GIRAFFE data with $R \approx 20000$ and $S/N \approx 50\text{--}100$, and approximately 150 clean and unblended lines around the 6300\AA region.

²⁰Using Calar Alto FOCES data with $R \approx 30000$ and $S/N \approx 50\text{--}100$, and a few hundred clean and unblended lines.

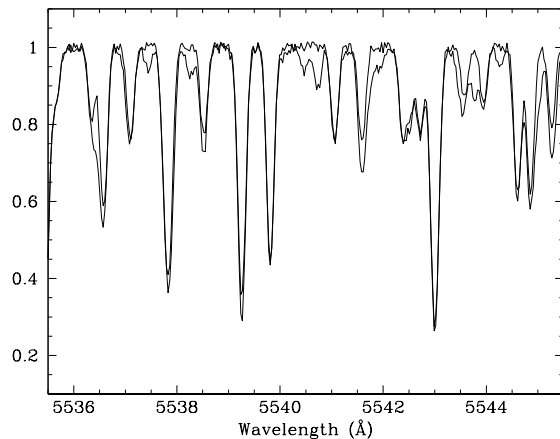


Fig. 5.— Artificial spectra used for continuum placement experiments, the *clean spectrum* (thin line) that includes only lines with EW between 20 and 100 mÅ, and the *full spectrum* (thick line), that contains also several hundreds of small lines with $EW < 20 \text{ mÅ}$, the vast majority having $EW < 1 \text{ mÅ}$.

were able to find the true continuum, when evaluating the area enclosed below the true continuum, we would not be measuring the flux of the intended transition alone, but its sum with all these other effects (Figure 4, Panels (a) and (b)).

Rather than trying to find where the true continuum lies, DAOSPEC looks for the *effective continuum*, a depressed continuum that takes into account, in a statistical sense, the unrecognized flux deficits and excesses due to all the sources described above²¹. Under the assumption that the unidentified and unrelated opacity sources underneath the spectral line in question are statistically similar to those lying at nearby wavelengths, DAOSPEC finds the effective local continuum by robustly balancing to zero the residual spectrum obtained after all the identified lines have been subtracted (Figure 4, Panel (c)). The area of a line measured with respect to the effective con-

²¹This is probably the reason why the *effective continuum* determined by DAOSPEC is sometimes lower than then continuum estimated by other programs, especially in the case of crowded spectra. Note however, that programs that rely on an automatic and *global* continuum placement procedure, like EWDET, tend to be always in good agreement with DAOSPEC, placing the continuum lower than *local* continuum estimates.

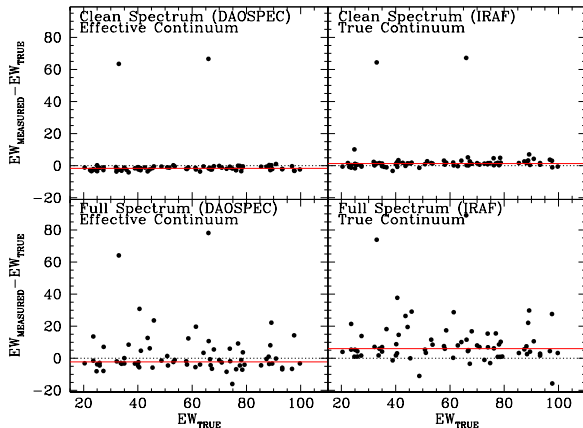


Fig. 6.— Difference between the measured and true (input) EW on the artificial spectra. The left panels show DAOSPEC measurements, based on the *effective continuum*, and the right panels IRAF *splot* measurements based on the *true continuum*. Top panels show measurements on the *clean spectrum* and bottom panels show measurements on the *full spectrum*. In each Panel, the dotted lines mark a perfect agreement ($\Delta\text{EW}=0$), while the solid lines mark the median ΔEW .

tinuum (Figure 4, Panel (d)) should be a more valid estimate of the correct EW of the particular atomic transition we are interested in, once the uncertainties of the procedure are properly taken into account.

3.2.1. Experiment with Artificial Spectra

We tested the above assertions with a simple experiment employing artificial spectra, created using a list of more than 1000 atomic lines belonging to 50 species, in the wavelength range 5500–5600 Å. The atomic data were obtained from the VALD²² database (Kupka et al. 1999). The most recent version of the spectral synthesis code originally described in Spite (1967) was employed, together with OSMARCS model atmospheres (Plez et al. 1992, and following updates), to predict the EW of each line for a metal-rich giant that should represent the typical difficult case: $T_{\text{eff}}=4500$ K, $\log g=1.0$, $v_t=1.0$ km s⁻¹, and $[M/H]=0.0$, with no α -enhancement. The artificial spectra were generated as simply as possible, simulating lines

with $\text{EW} < 100$ mÅ with saturated Gaussians (Section 3.3), and chopping out stronger lines (discussed in Section 3.3). A flat true continuum level was set to 1.0. The simulated spectral quality is typical of a modern echelle spectrograph, $\text{FWHM}=0.15$ Å ($R \simeq 40,000$), $S/N=35$, a scale of 0.03 Å/pixel. Two different spectra were generated (Figure 5): a *clean spectrum*, where all lines smaller than 20 mÅ were omitted, and a *full spectrum* including all lines, even the hundreds of tiny lines measuring as little as a fraction of a mÅ.

The same list of 86 lines was then measured on both the *clean spectrum* and the *full spectrum*: once with DAOSPEC relative to its estimate of the effective continuum, and again with the task *splot* in IRAF relative to the true continuum, which is exactly known and fixed to 1.0 in this ideal case (see Figure 5). Results are presented in Figure 6. As anticipated, DAOSPEC’s effective continuum is lower than IRAF’s—by 1% in the clean spectrum and by 2.5% in the full spectrum. Both differences are smaller than the corresponding root-mean-square residuals estimated by DAOSPEC, which are 2.4% per pixel for the clean spectrum and 2.9% per pixel for the full spectrum. Since the simulated noise was the same in both spectra, the slightly higher variance measured in the full spectrum is presumably due to the hundreds of additional small, unresolved lines that it contained.

Both methods of measurement gave similar results on the *clean spectrum* (top panels of Figure 6): lines measured with respect to the effective continuum by DAOSPEC were underestimated by $\Delta\text{EW}=-1.60 \pm 0.95$ mÅ while lines measured with respect to the true continuum by IRAF/*splot* were overestimated by $\Delta\text{EW}=1.45 \pm 0.95$ mÅ. Both differences are probably negligible compared to the uncertainties involved ($\sim 1.5\sigma$).

When considering the *full spectrum* however, apart from an overall increase in the spread of the measurements, we find that the DAOSPEC measurements relative to the effective continuum remain closer to the input values and more consistent with the measurements on the *clean spectrum* than the IRAF/*splot* measurements with respect to the known true continuum. Specifically, we find net shifts of $\langle \Delta\text{EW} \rangle = -2.3 \pm 5$ mÅ for DAOSPEC/effective continuum and $\langle \Delta\text{EW} \rangle = +6.0 \pm 5.7$ mÅ for *splot*/true continuum. We as-

²²<http://www.astro.uu.se/~vald/>

sert, therefore, that as crowding increases, measurements relative to the true continuum—even when it is known perfectly—become unreliable because of the likelihood of including opacity contributions from unrecognized and unrelated spectral lines in the EW measurement for the target line²³.

This is especially important to consider when one is measuring EW interactively with packages such as IRAF, MIDAS or SPECTRE. The procedure of readjusting the continuum locally around the line can produce a systematic bias if the user tries to ignore weak spectral lines in the continuum samples by favoring the highest points in the spectrum or by selective placement of the continuum-sample endpoints; this fails to allow for the possibility that flux may be removed by similar uninteresting but nevertheless real absorption features occupying the same wavelength range as the line of interest. The depression of the continuum by such weak lines is, in fact, very difficult to estimate in an impersonal and repeatable way by eye when using only small regions around each line. However, we believe that we can reduce the systematic errors due to unrecognized absorption features by iteratively using our model profiles to subtract all recognized spectral lines and then running the estimated continuum through the middle of the remaining flux spectrum, taking this to represent the typical local flux per pixel in the presence of all *unmodeled* opacity sources.

3.3. EW Gaussian Fit

When measuring EWs, DAOSPEC applies to crowded stellar spectra a concept also used in the analysis of crowded stellar images (e.g., DAOPHOT and ALLSTAR, Stetson 1987), i.e., the idea of fitting small groups of features simultaneously. This concept is used also in the interactive deblending routine of the IRAF task *splot*, but to our knowledge has not been implemented in an automatic program up to now. Besides allowing each absorption feature to be responsible for its own fraction of the flux missing from individual pixels, another advantage of this approach is that

the fitting function of each feature now does not need to be truncated close to the feature center, but can extend outwards by several pixels (e.g., up to 6σ for a Gaussian function, where the intensity of a line is down by a factor $e^{-18} \sim 10^{-8}$ from its maximum value), even in those regions where it overlaps one or more nearby features. Deblending as in DAOSPEC can therefore be more effective than in those programs that fit lines individually.

The fitting function employed in DAOSPEC is based on a *saturated Gaussian*²⁴ defined as

$$h(\lambda) = \frac{g(\lambda)}{1 + g(\lambda)} \quad (7)$$

where $g(\lambda)$ is the Gaussian function (Equation 2). This particular formulation was chosen because deviations of $h(\lambda)$ from the original Gaussian shape are only important for strong lines: accordingly, as $g(\lambda)$ becomes small $h(\lambda)$ tends to $g(\lambda)$. Furthermore, this formula ensures that the residual flux at line center ($\sim 1 - h(\lambda)$; cf. Eq. 3) approaches zero asymptotically as the EW grows without limit; if a pure Gaussian function had been retained as the model spectral line, there is no mathematical principle that prohibits the line profile from crossing over into negative fluxes ($A > 1$ in Eq. 2) as the line strength increases. Clearly, our adopted numerical formulation is not justified from physical first principles, but it is found empirically that it provides a useful extension of the general method to moderately saturated lines. It cannot, of course, adequately reproduce lines that are strongly saturated. The exact EW at which the method is no longer valid clearly depends on the spectral resolution and S/N ratio, since the better a spectral line is defined, the more statistically significant its deviation from the model profile will be²⁵.

²³In reality, since perfect knowledge of the true continuum position in real—as opposed to simulated—spectra is impossible, a person who attempts to estimate the true continuum level to anchor EW measurements risks a systematic error that is probably somewhere between the two limiting cases shown here.

²⁴In the future, when higher resolution spectrographs will become routinely available, we plan to update DAOSPEC so that the user will be able to choose among different fitting profiles, including the Voigt profile, that would take care of lines with extended wings. It should be noted that these extended wings will substantially increase the analysis times which may, we hope, be ameliorated by faster computers.

²⁵Of course, not all lines deviate perceptibly from the adopted profile at exactly the same EW, since the line profile, and in particular the extended line wings, depend on the physical properties of the particular transition that produces the line.

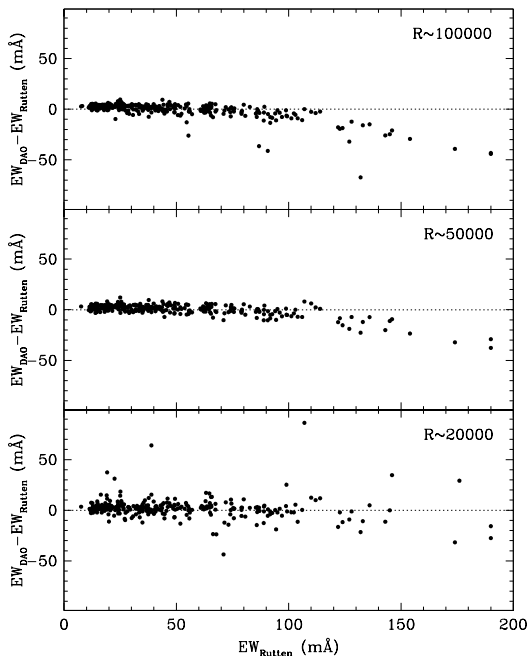


Fig. 7.— Comparison between DAOSPEC measurements and EWs by Rutten & van der Zalm (1984) on the UVES Solar spectrum for three different resolutions: $R \sim 100000$ (top panel), $R \sim 50000$ (middle panel) and $R \sim 20000$ (bottom panel). The EW at which the Gaussian approximation adopted by DAOSPEC is no longer valid appears clearly as that EW where ΔEW starts to deviate from zero.

To test how well our Gaussian approximation holds for real spectra, we have used the UVES Solar spectrum²⁶, which has an intrinsic resolution of about $R \sim 10^5$; we have also degraded it to resolutions of $R \sim 50000$ and $R \sim 20000$. We have measured EW with DAOSPEC using the list of clean Solar lines by Rutten & van der Zalm (1984). The difference between measurements by DAOSPEC and by Rutten & van der Zalm (1984) is shown in Figure 7 for the three Solar spectra. As can be seen, for the two high resolution cases DAOSPEC measurements begin to deviate from those of Rutten & van der Zalm (1984) at around 80–90 mÅ (for $R \sim 10^5$) and 100–120 mÅ (for $R \sim 50000$),

while the agreement remains within the noise up to ~ 200 mÅ in the lowest resolution case.

Another feature of DAOSPEC that helps deblending in crowded spectra is the fact that the FWHM is consistent for all lines, instead of being left as a free parameter in the fit of each individual line, as was already discussed in Section 2.1. Either the FWHM is forced to be the same for all lines, or it can scale with wavelength, which is more appropriate for echelle high-resolution spectra that have been rebinned in wavelength. A first guess at the FWHM is input by the user and it is subsequently refined during the robust least-squares fits that take place in the main loop of DAOSPEC (central part of Figure 3).

An additional advantage of the way DAOSPEC works again relates to the measurement of strong features in crowded spectra. For interactive routines trying to fit each absorption line separately, the safe region is generally limited to the line core, which is most often approximately Gaussian. This leads to an underestimate of the EW of strong lines that have an important flux contribution in their (non-Gaussian) wings. DAOSPEC fits lines by minimizing the residuals over the entire line profile after all fitted lines have been subtracted: the *total* area of the residuals is forced to be as close to zero as possible (an oversubtracted core forced to balance undersubtracted wings), and the total EW is still approximately correct to first order even if the line profile deviates from the adopted shape. This results from the fact that the whole line, including its extended wings, is included in the fitting region. Of course, as already noted, very strong lines cannot be properly measured this way.

3.4. Uncertainties

DAOSPEC provides three pieces of information that can be used to characterize the uncertainty of each EW measurement, described in the Sections below.

3.4.1. Formal Standard Error

The first is the formal standard error, $\sigma(EW)$, obtained during the least-squares determination of the EW of each line. This is a purely empirical $\sim 68\%$ confidence interval on the derived value of the line’s EW, derived from the standard deviation of the local flux residuals remaining af-

²⁶http://www.eso.org/observing/dfo/quality/UVES/pipeline/Solar_spectrum.html

ter the fitted continuum and all detected lines have been removed from the observed spectrum. Like EW, this has units of wavelength and results from a standard least-squares propagation of errors that weights the residual of each individual pixel according to that pixel's contribution to the determination of the line's EW. The relative error $\sigma(\text{EW})/\text{EW}$ can be used as an effective means of distinguishing good and bad lines, as shown in the top panel of Figure 8. Weaker lines have increasingly large relative errors, as expected due to the presence of noise and random blending. When the error rises above, say, 20% the lines could be considered unsatisfactory and could be omitted from an abundance analysis²⁷. Another way of using the relative error given by DAOSPEC would be to derive the abundance of one particular element not as a straight average of the single-line abundances, but as a weighted average, using $\sigma(\text{EW})d(\text{abundance})/d(\text{EW})$ to define the weights.

3.4.2. Quality Parameter

The second is called the *quality parameter* Q , and is also associated with each individual EW measurement. For each line, the root-mean-square value of the intensity residuals is calculated for the same range of pixels as were employed in the profile fit for that line. The ratio of this root-mean-square residual to the root-mean-square intensity residual for the spectrum as a whole is that line's Q value. Thus, it tells whether the particular region where that line sits is more ($Q > 1$) or less ($Q < 1$) problematic than the average for the spectrum as a whole.

The Q value for a given line can be higher than average if the line more strongly deviates from the Gaussian form than the average line, because in this case the local residuals will have a higher variance than the rest of the spectrum. This is illustrated in the middle panel of Figure 8, where the Q values of lines measured in star 2129 of the Open Cluster Cr 110 (from Pancino et al., in preparation) are plotted as a function of EW. As can be seen, most lines above 200 mÅ have $Q > 1$, that is, the residuals near their positions are higher than the average residuals for other parts of the spectrum.

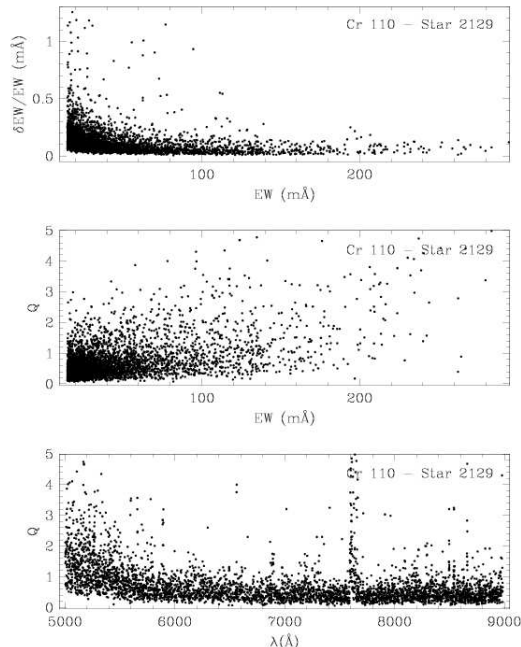


Fig. 8.— Behaviour of the relative error $\Delta\text{EW}/\text{EW}$ as a function of EW (top panel) and of the quality parameter Q as a function of EW (middle panel) and λ (bottom panel). The plot reports DAOSPEC measurements for star 2129 in the Open Cluster Cr 110 (from Pancino et al., in preparation).

Another reason why Q could be higher than average is that the spectral quality (crowding, S/N ratio, defects) is not homogeneous along the whole wavelength interval. In the bottom panel of Figure 8, Q is plotted as a function of wavelength. As can be seen, lines at the blue end of the spectrum—where the S/N ratio is lower than in the rest of the spectrum—tend to have higher Q values than the rest. Also, the region around 7600 Å tends to have bad Q values due to the telluric absorption band of O_2 . In some cases (i.e., strongly varying S/N ratios) these effects could be alleviated by adopting different Q selections for different spectral regions. In some other cases (anomalous crowding, defects or molecular bands), it could be safer to cut out the whole region in λ where anomalous Q values are clustered.

As a general rule, therefore, a lintel in Q can

²⁷As a rule of thumb, lines with EW smaller than three times $\sigma(\text{EW})$ should certainly be rejected.

be defined, depending on the particular spectrum, to reject less reliable measurements. In the case of Figure 8, for instance, some value $1 \lesssim Q_{\text{lim}} \lesssim 2$ could be adopted depending on the specific goals of the abundance analysis. However, please note that if a too strict selection in Q is adopted, some systematic effects could be introduced in the analysis that are difficult to foresee. Perhaps safer would be simply to increase the adopted $\sigma(\text{EW})$ values for lines with moderately large values of Q in the ensuing abundance determinations.

3.4.3. Standard deviation of Residuals

The third parameter, which characterizes the quality of the solution as a whole and is given in the header of the output file, it is the standard deviation of the flux residuals, which can be constructed as the r.m.s. relative (percentage) scatter in the effective continuum on a pixel-by-pixel basis. This has units of flux, and is mainly due to photon noise in the spectrum, of course, but substantial contributions can also come from unrecognized weak lines and molecular bands, which are generally more important in metal-rich, cool, and/or low-gravity stars, or from imperfections of the instrument or in the preliminary analysis, such as in the merging of echelle orders, the subtraction of night-sky emission lines, or the removal of CCD fringing effects. Note that since this index represents a pixel-by-pixel residual variance about the adopted mean continuum, positive and negative EW errors should occur with similar frequency, and the overall error in the abundance of any given atomic species, due to these effects, should decline with increasing numbers of lines measured, especially if the lines span a large wavelength interval.

To evaluate the likely impact on the EW results due to the overall, *systematic* uncertainty of the continuum placement, a few considerations can be useful. First of all, the *absolute* uncertainty of the continuum level, in flux units, must be at least as large as the standard deviation of the flux residuals divided by the square root of the number of pixels:

$$\sigma(I_C) \geq \frac{\sigma(1 \text{ pixel})}{\sqrt{N}}$$

Since it is often more convenient to work in relative units, with $\sigma(1 \text{ pixel})/I_C$ representing the *fractional* standard deviation of the flux residuals,

$$\frac{\sigma(I_C)}{I_C} \geq \frac{\sigma(1 \text{ pixel})/I_C}{\sqrt{N}}$$

gives a lower limit to the *relative* uncertainty of the continuum placement.

However, the N pixels have been used to derive a model continuum consisting of a polynomial of n^{th} order, i.e., to determine $n+1$ free parameters. To be ultraconservative, the pixels that are covered by spectral lines could also be entirely omitted from the uncertainty computation. Therefore, if n_l is the total number of lines found by DAOSPEC and n is the polynomial order, the ultraconservative estimate of the uncertainty of the global continuum placement procedure is

$$\frac{\sigma(I_C)}{I_C} \lesssim \frac{\sigma(1 \text{ pixel})/I_C}{\sqrt{\frac{N-(n_l \cdot \text{FWHM})}{n+1}}}. \quad (8)$$

where we have supposed that each of the $n+1$ parameters of the continuum model is independently determined from at most $\frac{N}{n+1}$ pixels. For instance, in a modern spectrum containing 40,000 pixels (N) and 1,000 spectral lines (n_l), having a FWHM of 10 pixels and a continuum shape corresponding to a 20^{th} -order polynomial, and producing a residual spectrum with a noise level of 1% (per pixel, root-mean-square), the overall uncertainty in the continuum placement cannot be as good as $1\%/\sqrt{40000} \approx 0.005\%$, but neither is it likely to be as bad as $1\%/\sqrt{\frac{40000-(1000)(10)}{21}} \sim 0.03\%$. The global impact of this continuum uncertainty on the EW results can be estimated by comparing a relative standard error calculated in this way to the typical biases illustrated in Fig. 2 above. Alternatively, the spectrum, normalized with the continuum produced by DAOSPEC, can be multiplied by the corresponding $1 - \Delta I_C/I_C$ and by $1 + \Delta I_C/I_C$ and the two spectra thus obtained can be fed to DAOSPEC while switching off the continuum-fitting procedure (ORDER=-1). The difference between the two sets of EW and the original DAOSPEC result will give a more precise evaluation of the systematic uncertainty in the EWs due to the continuum placement procedure.

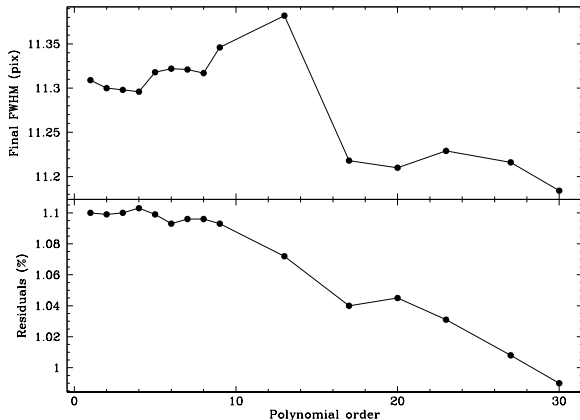


Fig. 9.— An example that shows how the final output FWHM varies with the Legendre polynomial order (top Panel) and how the residuals of the subtracted spectrum (bottom Panel) vary with the Legendre polynomial order.

3.5. Dependency on Input Parameters

In this section we perform a few experiments to show how the results of DAOSPEC depend on the most relevant input parameters. A detailed description of the parameters can be found in the DAOSPEC Cookbook (Pancino & Stetson 2008), here we describe only the ones that have the most impact on the EW results.

3.5.1. Polynomial Order for Continuum Fit

As already mentioned in Sections 2, 2.2 and 3.2, overall continuum placement has a global and systematic impact on the EW measurements. The only user-specified DAOSPEC input parameter that directly regulates it is the order of the Legendre polynomial used. This has little impact on the *average* continuum level because there are no other rejection or tweak parameters that alter the fit (see Section 3 for a description on how the continuum is fit). This is illustrated in Figure 9, where a sample spectrum has been fitted with different-order polynomials and the effect on the output FWHM and residuals of the subtracted spectrum has been shown. In general the FWHM changes are erratic, while the average residuals decrease when the polynomial order increases.

To choose the appropriate order for the continuum fit, a good rule of thumb is to compare the

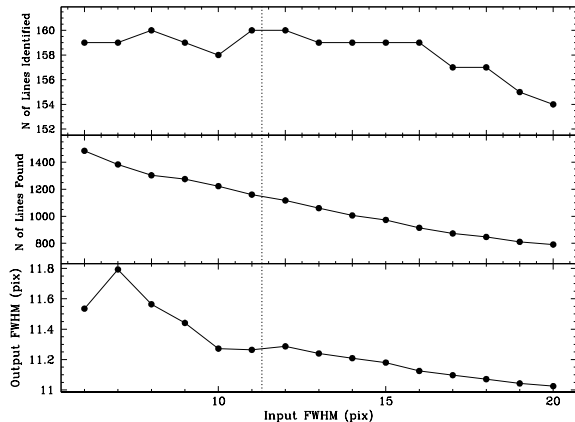


Fig. 10.— The three panels show (from top to bottom) how the number of lines identified in the input line list varies with the input FWHM, how the total number of lines found varies with the input FWHM and how the final output FWHM varies with the input FWHM. The dotted lines mark the correct FWHM=11.3 pixels.

scale length of the global variations in the spectral shape to the total spectrum length. If the variations are frequent and happen down to a scale length of $1/m$ of the total length of the spectrum, then the appropriate order to choose is m . If too low a value of m is adopted, there will be regions of the spectrum where the continuum is overestimated and other regions where it will be underestimated, leading to an increase in the scatter of the resulting EWs (see also Section 4.1.2). For chemical species whose abundances rely on only a few lines, the mistake can be significant. On the other hand, provided that the spectrum contains many, many more than m valid pixels (which should normally be the case) the main risk in adopting too *large* a value of m would be some increase in the reduction time. In case of doubt, we recommend that the optional output spectrum containing the fitted continuum be produced and overplotted on the original spectrum with, e.g., IRAF to check whether the order has been chosen appropriately (see also Figure 17).

3.5.2. First-Guess FWHM and Scaling

DAOSPEC needs a first guess for the FWHM (in pixels) to be able to initially distinguish and

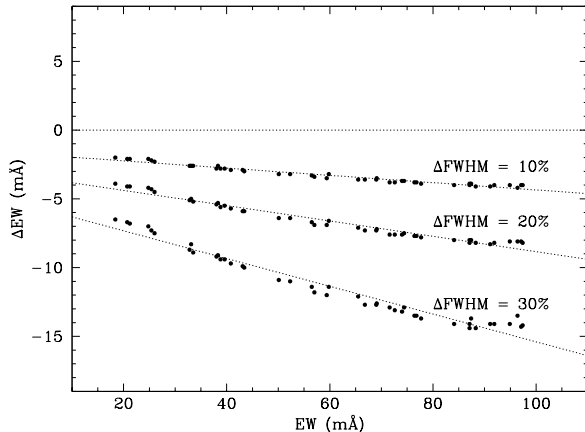


Fig. 11.— A spectrum with a $\text{FWHM} \simeq 5$ pixels is measured with DAOSPEC using a FWHM which is underestimated by 10%, 20% and 30%.

ignore features that are either too narrow or too broad to be likely real astrophysical spectral lines (see Section 3). Figure 10 shows what happens when the input FWHM is wrongly estimated by a large factor: while the number of detected lines that also appear in the input line list does not change very much, there is a significant change in the total number of lines found by the code; presumably this is because the input list contains primarily “interesting”—i.e., relatively strong—features, and it is the discovery of weak, mostly anonymous lines that is sensitive to the assumed FWHM. Since the working line list is limited to those lines detected initially, non-detection of real lines caused by initially specifying too large a FWHM is not fixed during the program’s main iteration loop. However, spurious detections occasioned by the initial assumption of too small a value of the FWHM may be rejected later on, as the FWHM and the EWs are refined. We find that the *output* FWHM does not change significantly if the *input* FWHM is wrong by one pixel (in this case, $\sim 10\%$), but starts to be over/underestimated perceptibly when the input FWHM is wrongly estimated by more than that. Comparing the *input* and the *output* FWHM after a first run of the code can help in deciding whether the reduction should be reformed with a different input FWHM.

The characteristic FWHM of a spectrum is often considered of secondary importance: we are not usually interested in its value except as it re-

lates to the quality of the EWs that are the principal goal of the analysis. However, DAOSPEC could be used to estimate the FWHM of a spectrum, which is extremely useful for spectral synthesis. While we have seen (Section 2) that a wrong *average* level of the continuum produces a *systematic offset* of the EW that does not depend strongly on EW, we show here that a wrong fitted value of the FWHM produces a *systematic trend* in the EW that depends on the EW itself. Figure 11 illustrates the difference in the EW on lines measured on the *clean spectrum* described in Section 3.2.1 and Figure 5, when the input FWHM is kept fixed to a wrong value, i.e., underestimated by 10%, 20% and 30%²⁸. Therefore, if the FWHM to which DAOSPEC converges differs by more than approximately 10% from the user input FWHM, the measurement should be repeated until the input and output FWHM are sufficiently similar.

One other important point to keep in mind is that in an echelle spectrum, where $\lambda/\delta\lambda$ is constant and the pixels are rebinned linear in wavelength, the FWHM changes from the blue to the red side of the spectrum. DAOSPEC allows the use of a constant FWHM or of a FWHM that scales with wavelength. Choosing a constant FWHM on an echelle spectrum would produce an overestimate of the FWHM in the blue and an underestimate on the red, with only the central EWs measured properly. This is illustrated in Figure 12, where the echelle spectrum of star 2129 in Cr 110 (Pancino et al., in preparation), ranging from 5500 to 6900 Å, is measured without scaling the FWHM and compared with the correct measurements where FWHM is scaled. As can be seen, the longer the spectrum, the bigger the mistake, which can be of a few mÅ. When the EW differences are plotted as a function of wavelength (top panel), we see a clear trend, with an increase of the spread on the sides, while when they are plotted as a function of EW (bottom panel) the only noticeable effect is an enormous increase in the spread.

²⁸Please note that in this case, unlike in Figure 10, both the *input* and *output* FWHM are wrong, i.e., we force DAOSPEC to use the wrong values by setting `FIX=1`

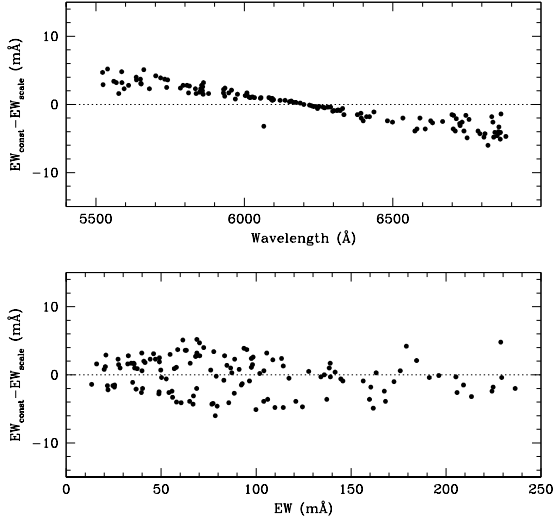


Fig. 12.— EW difference on measurements done with constant FWHM and with FWHM scaled with λ on an echelle spectrum of Star 2129 in Cr 110. In the top panel ΔEW is plotted versus wavelength, showing how EWs are overestimated in the blue and underestimated in the red. In the bottom panel ΔEW is plotted versus EW, where the mistake appears as an extremely large scatter.

3.5.3. Residual Core Flux

In real stellar spectra, the center of a line is never completely black because the effective surface of a stellar atmosphere is not at a temperature of absolute zero. Even strongly saturated lines, such as the H_α line (at 6563 Å) in the spectrum of a low mass red giant, never reach zero flux even in their cores. Telluric absorption lines (i.e., the O_2 and H_2O bands) or interstellar absorption lines (e.g., the NaD doublet) can, on the other hand, be much darker in their centers. Depending on the resolution and pixel size of a particular spectrum, the maximum depth of strong lines varies a bit. For example, the spectrum of Figure 13 has an H_α line that reaches 20% of the continuum value in the line core. This effect is modeled in the DAOSPEC analysis by a further simple modification of Eq. (6) above: the model line profile now becomes

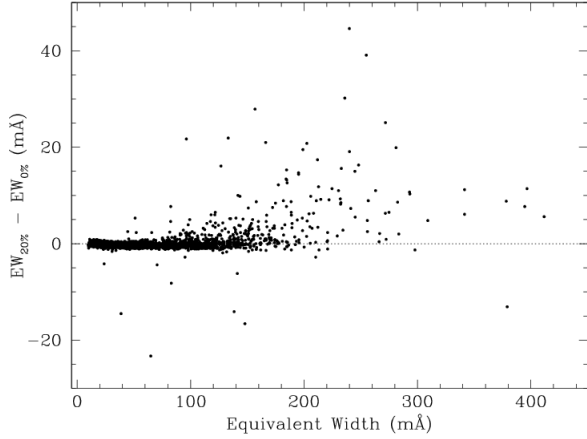


Fig. 13.— EW difference on measurements done with the correct Residual Core Flux value of 20% and the wrong value of 0%. The largest differences appear of course for strong lines.

$$f(\lambda) = \frac{g(\lambda)}{1 + g(\lambda)/(1 - \rho)} \quad (9)$$

The model of the spectrum in the region of the line then becomes

$$I(\lambda) = I_C \cdot (1 - f(\lambda)) \rightarrow \rho I_C$$

as $g(\lambda) \rightarrow \infty$. The quantity ρ , known as the “residual core flux,” is specified by the user and is typically in the range 5–25%. It ensures that the profiles of strong lines saturate to a value equal to some fraction of the local continuum flux I_C rather than to a value of zero. A side-effect of this saturation model is that as lines become stronger within the saturation regime, they also become broader even for a fixed value of the FWHM parameter. This improves to some extent the capability of the model line profiles to mimic the actual profiles of real spectral features.

3.6. Dependency on Spectral Quality

To test the effect of the spectral quality on the EW measured by DAOSPEC, we created different versions of the *full spectrum*, our most crowded artificial spectrum described in Section 3.2.1, with different S/N ratios, resolution ($R = \lambda/\delta\lambda$), and pixel sampling.

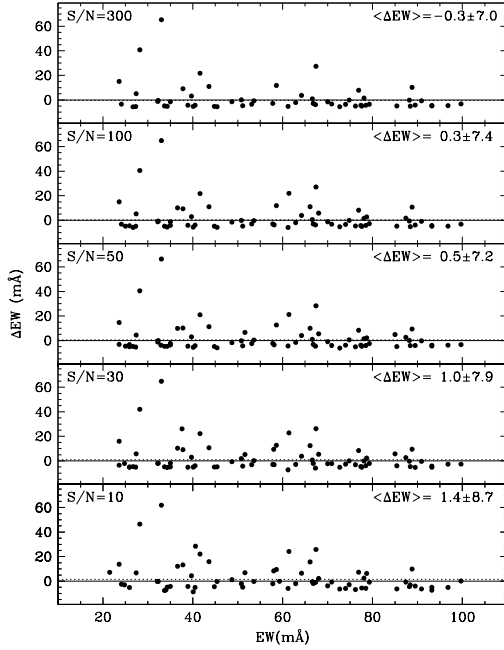


Fig. 14.— Difference on the EW measured with DAOSPEC and the “true” input EW of five artificial spectra with $R = 35000$ and S/N ratios ranging from S/N= 300 (top panel) to S/N=10 (bottom panel). Continuous lines mark perfect agreement and dotted lines the σ clipped average, also indicated on the top of each panel.

3.6.1. S/N Ratio

The first experiment is shown in Figure 14, where the difference between the EW measured by DAOSPEC and the *known* input EW is plotted versus EW for five artificial $R \simeq 35000$ spectra at various S/N ratios and with a sampling of approximately 5 pixels for each resolution element. Mean (σ -clipped) values with their line-by-line variance (σ) are reported in Figure 14. As can be seen, there is no significant variation of the average ΔEW , which always remains close to zero, within the uncertainties. The variance σ increases by approximately 2 mÅ from the S/N=300 to the S/N=10 case, as expected. Therefore, DAOSPEC gives good results even with a S/N ratio as low as 10. This is due in part to the fact that the FWHM

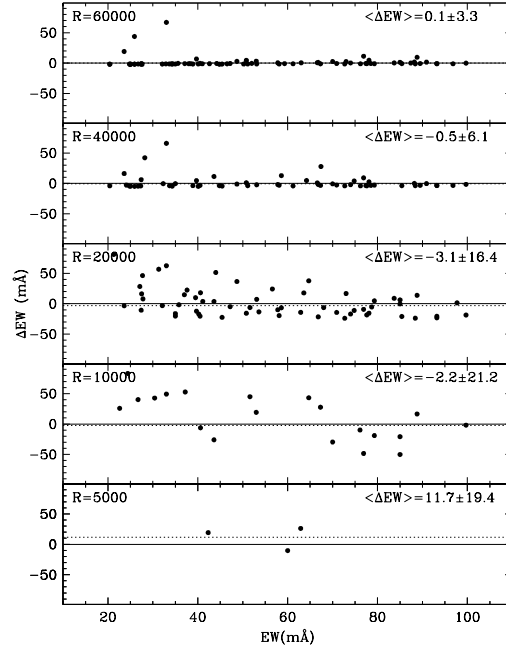


Fig. 15.— Difference on the EW measured with DAOSPEC and the “true” input EW of five artificial spectra with S/N=100 and resolution ranging from $R=60000$ (top panel) to $R=5000$ (bottom panel). Continuous lines mark perfect agreement and dotted lines the σ -clipped average, also indicated on the top of each panel.

used by DAOSPEC is the same²⁹ for all lines: if the spectra are properly sampled³⁰, DAOSPEC can usually tell a line from a noise feature. This result is somewhat in contradiction with a similar experiment performed by Sousa et al. (2006), and described in detail in Section 4.1.2.

3.6.2. Resolution

Resolution appears to be more critical than the S/N ratio as can be seen in Figure 15, where five spectra of fixed S/N=100 and similar sampling of approximately 5 pixels have been created at R ranging from 5000 to 60000. Again, the average σ -clipped difference between DAOSPEC measurements and the “true” input EWs are always

²⁹Scaled with wavelength in the case of echelle spectra.

³⁰at least 2 pixels per resolution element.

consistent with zero within the spread. However, for $R=5000$, the total number of identified lines is very low. This, of course, is inherent to the intrinsic quality of the spectra and not necessarily specific to the algorithms employed in DAOSPEC. Nevertheless, $R=10000$ can perhaps be considered a lower limit of validity of the EW method in general, and of the use of DAOSPEC in particular. We expect that stars with very high rotation velocities will behave as if they had a lower instrumental resolution, as a consequence of the correspondingly broad line profiles.

When resolution reaches $R \simeq 40000$, ΔEW gets definitely better not only in terms of the average, but also in terms of the spread, which at $R=60000$ becomes $\simeq 3 \text{ m}\text{\AA}$. However, we must reiterate that our artificial spectra are simplistic, because all the simulated lines have pure Gaussian profiles. In real spectra, the effect of non-Gaussian wings on strong lines becomes important, as has been discussed in Section 3.3 and shown in Figure 7.

3.6.3. Pixel Sampling

The last factor that may have an impact on EW measurements is the pixel sampling of the resolution element. The Nyquist-Shannon Theorem (Shannon 1949) states that the reconstruction of a continuous signal from its samples is possible if the signal is bandlimited and the sampling is greater than twice the signal bandwidth. In our case, the adequate reconstruction of a line profile is only possible if it is sampled by at least two pixels.

Figure 16 shows the usual comparison between DAOSPEC measurements and “true” input EW on five artificial spectra with fixed $R=35000$ and $S/N=100$, and different sampling ranging from 10 pixels (FWHM) to 1 pixel. As can be seen, all cases with $\text{FWHM} \geq 2$ pixels are comparable to each other, with the average ΔEW practically equal to zero and $\sigma \simeq 8\text{--}9 \text{ m}\text{\AA}$. In the case of $\text{FWHM}=1$, the spread in ΔEW is naturally much higher, while the average ΔEW remains reasonably close to zero. But a trend with EW seems present, in the sense that smaller lines tend to be slightly overestimated in a regime of under-sampling³¹.

Since noise introduces variations at the pixel

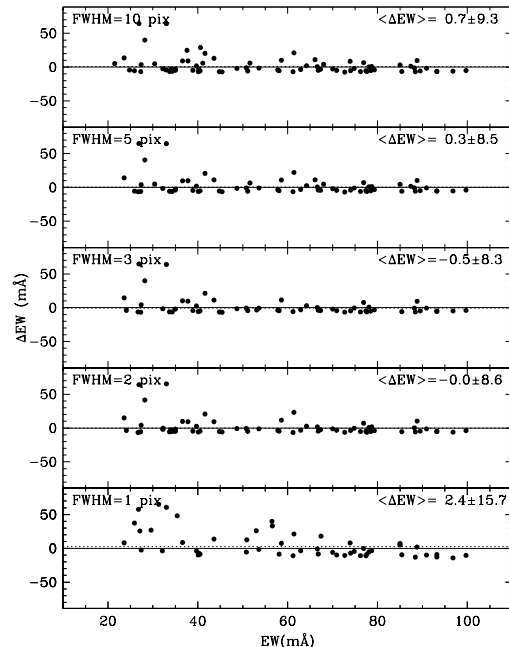


Fig. 16.— Difference on the EW measured with DAOSPEC and the “true” input EW of five artificial spectra with $S/N=100$, $R=35000$ and pixel sampling ranging from $\text{FWHM}=10 \text{ pix}$ (top panel) to $\text{FWHM}=1 \text{ pix}$ (bottom panel). Continuous lines mark perfect agreement and dotted lines the σ clipped average, also indicated on the top of each panel.

level, whenever the sampling is close to the under-sampling limit (2 pixels), it is possible that DAOSPEC starts confusing noise with features, thus increasing the variance of measurements as in Figure 16 (bottom panel). Otherwise, the use of a correct first guess of the FWHM improves the separation of noise from real features.

To summarize, DAOSPEC produces reliable results for spectra that are adequately sampled, but the possibility of using DAOSPEC to measure EW also in spectra that are undersampled appears promising, although with a higher uncertainty (especially for weak lines).

3.7. Performance considerations

As an automatic program, DAOSPEC is fast if compared to interactive or semi-automatic pro-

³¹This could be due to a larger uncertainty of the FWHM estimate in a regime of undersampling.

grams, especially when used in batch mode and without the graphical interface. However, given the large computational power of modern machines, and given that it can be run 24 hours a day, 7 days a week without full-time supervision, DAOSPEC has been designed to give the most accurate results possible rather than the fastest possible execution. In particular, the five big loops described in Figure 3 can take a long time in the interest of obtaining more reliable continuum placement, FWHM estimate, and line parameters.

A few tests on different machines show that one spectrum can be measured in a short time, ranging from a few seconds to a few minutes, depending on the spectral quality and other factors that are described in detailed in the following Sections. As an example, DAOSPEC took a few minutes to measure 2429 line on the FEROS spectrum of Section 4.1.2 (190 000 pixels long), a Solar-type star with a crowded spectrum and a complicated continuum shape. The above test was done on a Mac Pro workstation, with a Dual-Core Intel Xeon Processor (2x2.66 GHz - 4 cores) and 2GB of RAM memory, and the Mac OS X version 10.4.11 (Tiger).

3.7.1. Major factors

The three major factors that have a large impact on the execution speed of DAOSPEC are the following:

- The MXSPEC parameter, within the main code file (`daospec.f`), specifies the maximum number of pixels in the spectra that will be analyzed. The higher this value, the larger the amount of computer memory reserved. Setting MXSPEC to unnecessarily high values can cause the code to go unbearably slow or even to crash on some machines;
- Setting the input FWHM to a severely wrong value can make the code go slower by a factor of 10 or even 100, as many executions of the inner iteration loops attempt to cope with the anomaly. We recommend deriving a robust estimate of FWHM before starting the computation, as suggested in the DAOSPEC Cookbook (Pancino & Stetson 2008);
- In general, the longer the spectrum (in pixels) and the larger the number of lines in the spectrum (not in the laboratory line list), the longer it takes for DAOSPEC to converge. In complicated spectra, setting a larger value for the smallest interesting EW can reduce the number of loops and make the code go faster, although MXSPEC and FWHM have a much stronger impact.

3.7.2. Secondary factors

Other factors to take into consideration, although they have a smaller impact (see the DAOSPEC cookbook, Pancino & Stetson 2008, for more details), are the following:

- Adroit use of the Fortran compiler can optimize the code for faster execution;
- Spectra with a simpler shapes, i.e., flatter continua, are faster to fit. Similarly, using a low continuum order (if appropriate) makes the computation faster, but it can also make execution significantly slower if used inappropriately (see Section 4.1.2). Also, setting the continuum ORDER=-1 (i.e., no continuum fit) can also speed up the computation if the user is satisfied that the spectrum has already been adequately rectified;
- Using a FIXED FWHM makes the computation a bit faster, but please see Figure 11 for the risks associated with a wrong FWHM estimate;
- Some very small improvement can also be obtained if the fixed FWHM option is used even for echelle spectra if they cover a very short wavelength interval, but at the expense of the EW accuracy (Section 3.5.2);
- Using a smaller interval for the radial velocity cross-correlation also makes the computation faster. Leaving the search interval to its default value ($\pm 500 \text{ km s}^{-1}$) is only advisable if there is no prior constraint on the approximate radial velocity of the objects;

4. Comparisons

In this Section we compare results produced by DAOSPEC with data and programs from the

current literature. We summarize and discuss all the papers that, to our knowledge, have made use of DAOSPEC in Section 4.1, including our own test with data from Pancino et al. (2002). We also compare DAOSPEC with EWDET (Section 4.2) and with ARES (Section 4.3) and we finally perform an abundance analysis of the Sun (Section 4.4).

4.1. Literature tests on DAOSPEC

DAOSPEC has been available to the astronomical community since 2002, when the first test versions were circulated. Since then, it has evolved into the form presented here and in the Cookbook (Pancino & Stetson 2008), and it has been used and tested by some colleagues: a few authors used the code without mentioning any specific tests (Meléndez et al. 2003; Pasquini et al. 2004; Dall et al. 2005a,b, 2006; Pompéia et al. 2005; Zoccali et al. 2006; Lecureur et al. 2007).

Other papers compare DAOSPEC measurements to manual measurements with IRAF, MIDAS or other methods and find a good agreement, but they do not explicitly show the comparison (Pancino 2004; da Silva et al. 2005, 2006; Barbay et al. 2006, 2007; Letarte et al. 2006; Letarte 2007; Alves-Brito et al. 2006). One paper used DAOSPEC to measure radial velocities and mentions that a comparison with the results of *fxcor* within IRAF gives agreement within the uncertainties (Monaco et al. 2005). Another couple of papers publish the comparison of EWs measured by DAOSPEC with manual measurements (Alves-Brito et al. 2005; Venn & Hill 2005); these are discussed in Section 4.1.1.

To our knowledge, only two papers test DAOSPEC extensively: Sousa et al. (2006) and Sousa et al. (2007), which are discussed in detail in the following sections.

4.1.1. Basic Comparisons

Alves-Brito et al. (2005) used DAOSPEC to measure EW of Fe I and Fe II lines in five red giants in 47 Tuc. A comparison of IRAF interactive measurements with DAOSPEC results on star 25 showed relatively good agreement, in the sense that the average ΔEW was smaller than the spread ($\sigma=4.82$ mÅ, see their Figure 3). But a slight trend with EW appeared, in the sense that

for larger EW the ΔEW became larger. According to the discussion in Section 3.5.2 above, an effect like this could, for instance, be due to a slightly ($\simeq 10\%$) inappropriate input FWHM, but we do not know whether something like that is in operation here. In the end, the authors chose to adopt the IRAF measurements to derive their atmospheric parameters and iron abundances.

Another, more favorable comparison was shown by Venn & Hill (2005), who plotted IRAF EW measurements by Shetrone et al. (2003) versus DAOSPEC, on GIRAFFE spectra ($R \simeq 20000$) of two stars in the Sculptor dwarf galaxy. They found good agreement (within 10%), with no sign of departures from the 1:1 relation for strong lines up to 200 mÅ. This is expected if one considers the example of Figure 7, where we show that the Gaussian approximation is more and more reliable, even for strong lines, as resolution goes down from $R \simeq 10^5$ to $R \simeq 20000$.

4.1.2. Detailed Comparisons

Only two papers have performed detailed tests on DAOSPEC, namely Sousa et al. (2006) and Sousa et al. (2007).

Sousa et al. (2006) used a synthetic (noiseless) model Solar spectrum of very high quality ($R \simeq 120000$ and $S/N \simeq 300$) to compare DAOSPEC and IRAF EW measurements. They found essentially perfect agreement in a red window (6000–6300 Å) with $\Delta EW = 0.8 \pm 1.1$ mÅ, based on 34 lines, and fair agreement in a blue window (4400–4650 Å) with $\Delta EW = 4.0 \pm 4.9$ mÅ, based on 25 lines (see also Figure 20). This must of course be due to the higher crowding level and lower S/N ratio of the blue part of the spectrum.

The synthetic spectrum was then degraded both in S/N ratio and resolution, and the DAOSPEC measurements were compared with each other. DAOSPEC appears to give very different average EWs and variance, by as much as $\Delta EW = 15 \pm 20$ mÅ, for the lowest resolution case ($S/N \simeq 10$ and $R \simeq 12000$). While some increase in the variance can be easily understood when varying S/N ratio or resolution, as can be seen in our own tests (Section 3.6), EW discrepancies and variance as large as those reported by Sousa et al. (2006) are difficult to understand, and indeed we do not find such behavior in our own tests (Sections 3.6.1 and

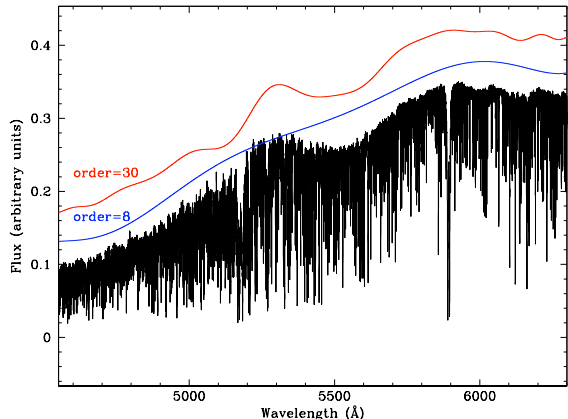


Fig. 17.— A typical FEROS spectrum of a Solar-type star (kindly provided by S. Sousa). Two Legendre DAOSPEC polynomials are overplotted, with an arbitrary vertical offset for clarity. As can be seen, the Legendre polynomial of 8th order (lower continuous line) does not adequately represent the spectral shape, while the 30th order polynomial (upper continuous line) fits the spectrum better.

3.6.2).

When measuring their FEROS spectra, Sousa et al. (2006) encountered some problems. In particular, they found an enormous, unacceptable spread in the resulting EWs, and they managed to obtain reasonable EWs only by cutting the spectrum into 100 Å segments and running DAOSPEC manually on each small piece. The ΔEW from IRAF measurements then went down from 12.1 ± 17.1 mÅ to 3.0 ± 4.7 mÅ (S. Sousa, private communication) but, of course, at the expense of execution time and humanpower (several hours). They kindly provided us with some of their FEROS spectra (Figure 17) and we have repeated their measurements. We found that using a different order for the continuum fit (30 instead of 8, Figure 17) and a different FWHM (14 instead of 5, Section 3.5.2, Figures 10 and 11) gave much better EWs and decreased the execution time by a factor of 50, roughly. We also tried cutting the spectrum into short pieces, both as a consistency check and to test the execution times, but we used shell scripts (Cookbook, Pancino & Stetson 2008) to run DAOSPEC automatically—in 10 minutes, total time (see Section 3.7)—on the various pieces: we obtained $\Delta\text{EW} = -4.1 \pm 4.3$ mÅ when using the

full spectrum, and $\Delta\text{EW} = -6.5 \pm 4.4$ mÅ when the spectrum was cut into 100 Å pieces.

The paper that introduced ARES (Sousa et al. 2007) was the second to perform a detailed check on DAOSPEC, using the same datasets as Sousa et al. (2006) and the same DAOSPEC configuration parameters. ARES is based on the IRAF task *splot*, and therefore the first comparisons made were between ARES and IRAF, and between DAOSPEC and IRAF. The results obtained with ARES were more similar to IRAF than the ones with DAOSPEC, supporting the conclusion that ARES is a very well designed extension of *splot*. We have seen, however, that the most important factor in these comparisons can be the way the continuum is chosen. In case of crowded spectra, we have claimed that the algorithm employed by DAOSPEC can give better results (Section 3.2.1), but since both IRAF and ARES are highly customizable in terms of continuum placement, we do not doubt experienced and careful users can obtain good results with those algorithms.

To summarize, an appropriate choice of the configuration parameters is crucial to obtain good results with DAOSPEC. The Cookbook (Pancino & Stetson 2008) provides practical and objective methods for finding the best values for these parameters, as well as the discussions and tests presented in Section 3.5 here.

4.1.3. Red Giants in ω Centauri

The dataset of EW measurements that Pancino et al. (2002) obtained with the IRAF task *splot* to derive abundances for six red giant stars in ω Cen constitutes a good testbed for DAOSPEC. The full data description can be found in the original paper; in short, the six spectra were taken with UVES at the Very Large Telescope in Paranal, Chile, with $R \simeq 45000$ and $S/N \simeq 100\text{--}150$ per resolution element, covering the range 5250–6920 Å. Stellar metallicities range from $[\text{Fe}/\text{H}] = -0.49$ to -1.20 , with temperatures around 4000 K and gravities of about 1 dex. The input line list contains 230 features of various elements, although only $[\text{Fe}/\text{H}]$, $[\text{Ca}/\text{Fe}]$, $[\text{Si}/\text{Fe}]$ and $[\text{Cu}/\text{Fe}]$ were published by Pancino et al. (2002).

We remeasured these spectra with DAOSPEC and compared the results (Figure 18). A total of 1150 lines were used in the comparison.

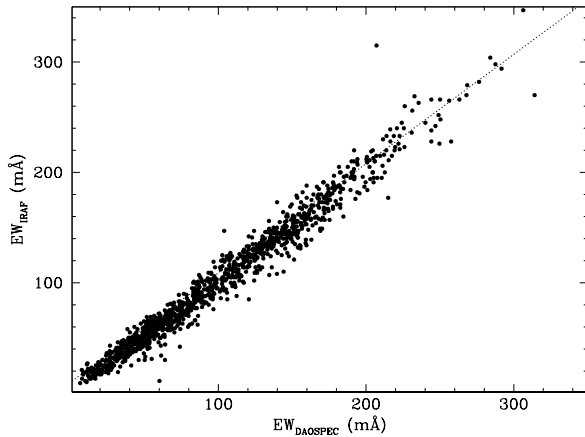


Fig. 18.— Comparison of the original measurements from Pancino et al. (2002), obtained with IRAF (Y axis), and the measurements obtained here with DAOSPEC with the same line list and on the same spectra (X axis). Perfect agreement is marked with a dotted line.

We found a very good average agreement, with DAOSPEC measurements marginally smaller, by $\Delta\text{EW} = -1.3 \pm 10.3 \text{ mÅ}$. When considering the six stars separately, we found differences ranging from $\Delta\text{EW} = -3.7 \pm 10.7 \text{ mÅ}$, for star WFI 222068, which is the most metal rich of the sample, to $\Delta\text{EW} = 1.1 \pm 7.1 \text{ mÅ}$, for star WFI 618854, which is the most metal-poor of the sample. No trend with EW is apparent.

The agreement appears satisfactory within the uncertainties, especially in the light of the tests performed in Section 3.2.1, where we show again that an agreement between DAOSPEC and IRAF measurements gets naturally worse as metallicity (and line crowding) increases.

4.2. DAOSPEC vs. EWDET

EWDET (Ramírez et al. 2001, see also Section 2) was obtained by courtesy of S. Ramírez. It came with a test spectrum of a moderately crowded red giant in M 71, covering the range 7900–8000 Å, with $R \simeq 30000$ and a S/N ratio of at least 100 everywhere. We used this spectrum with the default configuration file ewdet.inp provided with the code, to measure the EWs of 70 lines. Ten additional lines were found, but EWDET did not report an EW for any of them because the

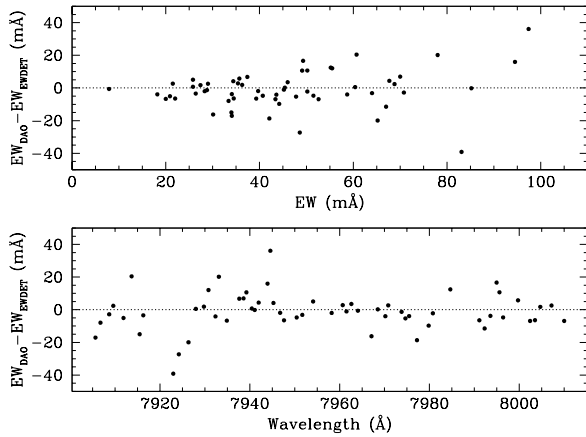


Fig. 19.— Difference between DAOSPEC and EWDET EWs measured on a test spectrum of a giant in M 71 provided with EWDET. ΔEW is plotted versus EW (top panel) and versus wavelength (bottom panel). The average difference is $\Delta\text{EW} = -1.2 \pm 11.7 \text{ mÅ}$.

Gaussian fit did not converge. All the lines found by EWDET were used as the input “laboratory” line list for DAOSPEC, which we then used to obtain EWs from the same spectrum. It is perhaps worth stressing here that the input line list plays no part in the *finding* of candidate spectral lines by DAOSPEC; it is only after features have been detected that tentative *identifications* with features in the input list are sought. There is no attempt to “force” the detection of features in the spectrum at wavelengths specified by the input laboratory list. In the present case, DAOSPEC was able to (independently) find and measure all the lines that EWDET had found, including the 10 that EWDET had subsequently discarded. No apparent defect was found on those 10 lines in a visual inspection of the spectrum.

Figure 19 plots the difference between the DAOSPEC and EWDET EWs versus EW (top panel) and versus wavelength (bottom panel). The average difference is $\Delta\text{EW} = -1.2 \text{ Å}$ with a variance of 11.7 mÅ . While the two sets of measurements appear in good agreement, the spread is slightly higher than expected, i.e., higher than that found in the comparison of Section 4.1.3 between DAOSPEC and hand-made IRAF measurements. A trend of increasing spread with increasing EW might be present, while no obvious trend with wavelength is seen.

A comparison of the model continua adopted by the two programs shows a an overall systematic difference of 1.3% (DAOSPEC continuum lower), with a variance of 0.6% around this mean offset. For comparison, the residual spectrum produced by DAOSPEC has a pixel-to-pixel flux variance of 2%. On the surface, this case appears to be similar to that discussed in Section 3.2 above. Such a discrepancy in the continuum levels could be the cause of the small ΔEW offset found between the two codes (see Section 2, Figure 2).

On average, the standard errors estimated by DAOSPEC are larger by $0.7 \pm 1.5 \text{ m}\text{\AA}$ than those reported by EWDET, even though the latter also includes the uncertainty due to the continuum placement and the former does not. In any case, given the large spread in ΔEW seen in Figure 19, both error estimates appear a bit small, indicating that some other unidentified source of uncertainty might be present. If we estimate an error budget, including the average errors by EWDET ($\sim 3 \text{ m}\text{\AA}$) and DAOSPEC ($\sim 4 \text{ m}\text{\AA}$) and an error due to the continuum placement as estimated roughly from Figure 2 ($\sim 7 \text{ m}\text{\AA}$), we account for a spread of $\sim 9 \text{ m}\text{\AA}$, i.e., the missing source of uncertainty must be of about $\sim 8 \text{ m}\text{\AA}$ ³². This might suggest that the EWDET continuum placement uncertainty (Ramírez et al. 2001, and Section 2.2 here) might be underestimated.

Finally the average difference between the FWHM found by EWDET for each line, and the FWHM found by DAOSPEC (scaled with wavelength) is $\Delta\text{FWHM} = 0.001 \pm 0.076 \text{ \AA}$, and the average radial velocity difference between the two sets, in the sense EWDET minus DAOSPEC, of measurements is very small, $\Delta v_r = 0.1 \pm 0.6 \text{ km s}^{-1}$.

Summarizing, the comparison can be considered satisfactory once all the sources of uncertainty are properly taken into account. The only minor disadvantage of EWDET is the fact that it has been written for personal use and it requires knowledge of Fortran to manually adapt some routines to meet the needs of each set of spectra, including naming conventions and so on.

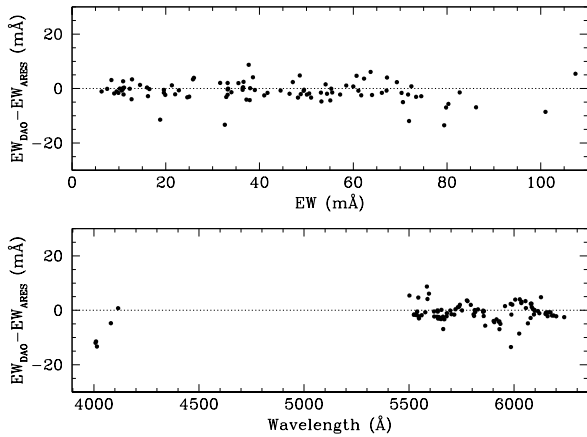


Fig. 20.— Difference between DAOSPEC and ARES EWs measured on a test spectrum of the Sun provided with ARES. ΔEW is plotted versus EW (top panel) and versus wavelength (bottom panel). The average difference is $\Delta\text{EW} = -1.1 \pm 3.7 \text{ m}\text{\AA}$.

4.3. DAOSPEC vs. ARES

ARES (Sousa et al. 2007) has been obtained from the ARES webpage³³ with, *inter alia*, a test spectrum of the Sun obtained with HARPS from observations of Ganymede³⁴. Similarly to what we have done with EWDET, we ran ARES on the test spectrum and used its output as an input line list for DAOSPEC.

The average differences of key parameters, in the sense of DAOSPEC minus ARES, can be summarized as follows: $\Delta\text{EW} = -1.1 \pm 3.7 \text{ m}\text{\AA}$, $\Delta\text{FWHM} = 0.01 \pm 0.05 \text{ \AA}$ ³⁵, $\Delta v_r = -0.002 \pm 0.126 \text{ km s}^{-1}$, based on 98 lines in common. No error estimate is provided by ARES. At first glance, all these values appear in very good agreement within the uncertainties, even better than the comparison made with EWDET in Section 4.2. This is especially

³²One thing to note here is that the spectral range chosen includes a relatively strong H₂O telluric absorption band, which could cause some of the observed scatter.

³³<http://www.astro.up.pt/~sousasag/ares/>

³⁴<http://www.ls.eso.org/lasilla/sciops/3p6/harps/monitoring/sun.html>

³⁵This difference is 100 times larger than in the case of the EWDET comparison. However, it corresponds to a $\simeq 8\%$ relative difference, which, according to our Figure 11, implies a ΔEW of a few $\text{m}\text{\AA}$ at most, compatible with the quoted $\Delta\text{EW} = -1.1 \pm 3.7 \text{ m}\text{\AA}$.

^sTable 1
Abundance Analysis of the Sun

EW	T _{eff} (K)	log <i>g</i> (dex)	<i>v_t</i> (km/s)	[FeI/H] (dex)	FeII/H] (dex)	<i>n</i> _{lines}
Moore et al. (1966)	5780	4.46	0.7	-0.012±0.005	+0.095±0.012	160
Rutten & van der Zalm (1984)	5780	4.43	0.8	-0.019±0.005	+0.010±0.013	197
DAOSPEC	5780	4.44	0.6	+0.005±0.008	-0.023±0.018	195

true when considering the spread in ΔEW , which is 11.7 mÅ in the comparison with EWDET and only 3.7 mÅ in the comparison with ARES. The very good agreement must of course be largely due to the fine quality of the test spectrum, which has $R \simeq 45000$ and $S/N \simeq 350$. Figure 20 confirms good agreement with no trends with wavelength or EW in the differences, except for a possible problem in the bluest and most crowded part of the spectrum. A last comparison was made on the number of lines found. The authors do not mention how many lines were found and/or identified by each code, but state that ARES finds more lines than DAOSPEC. If we compare the Solar spectra taken from Ganymede, we find that ARES identifies 101 lines, and DAOSPEC identifies 100.

ARES and DAOSPEC represent two very different ways of approaching the problem of measuring EWs. ARES closely follows IRAF, including a major IRAF feature, namely the possibility to customize the continuum fitting procedure. Because of the way the continuum is fit, ARES is faster than DAOSPEC, although maybe a bit longer to configure. ARES takes of the order of seconds for each spectrum, while DAOSPEC may take from a few seconds to a few minutes, depending on the spectrum characteristics. Finally ARES gives no error estimate or radial velocity; indeed, the radial velocity is one of the necessary inputs, not outputs of the code.

Nevertheless, in spite of the different continuum placement philosophies, ARES and DAOSPEC give entirely comparable measurements, within the uncertainties.

4.4. Abundance analysis of the Sun

As a final test, DAOSPEC was used on the Solar spectrum obtained with HARPS (Section 4.3)

to derive iron abundances for the Sun. The results have been compared, using the same models and abundance calculation code, to the abundances obtained with the EWs measured by Moore et al. (1966) and Rutten & van der Zalm (1984).

To measure EWs with DAOSPEC, we created a line list containing all lines in common between Moore et al. (1966) and Rutten & van der Zalm (1984). This line list was fed to DAOSPEC and, for homogeneity, it was also used to derive the Solar abundance with the original Moore et al. (1966) and Rutten & van der Zalm (1984) measurements.

We used the atmospheric models by Edvardsson et al. (1993) and the latest version of the abundance calculation code originally published by Spite (1967). For sake of homogeneity, the atomic parameters (including log *gf*) were taken from the line list of Rutten & van der Zalm (1984). In this way, the only difference among the three analyses comes from the EWs. The Solar temperature was kept fixed at 5780 K; gravity was allowed to vary between log *g*=4.4 and 4.5, to allow for micro-adjustments of the Fe I and Fe II ionization equilibrium; the micro-turbulent velocity was kept as a free parameter and the best value was chosen as the one that minimized the slope of the EW vs. [Fe/H] relation.

The results of our analysis are shown in Table 1, where it can clearly be seen that only negligible variations in log *g* and very small variations of the microturbulence (*v_t*) were necessary to obtain abundances that are quite compatible with each other, and with the Solar values.

5. Conclusions

While we have argued that one of the advantages of DAOSPEC is that it is minimally inter-

active, and hence fast and reproducible, we must confess that there still remain some user-specified reduction options whose best values are not entirely obvious. Examples of these are the polynomial order to be used in the continuum fits, the initial estimate of the FWHM value appropriate to a given spectrum, the range of plausible radial-velocity values to consider, and the minimum EW that is considered to be of interest. In some sense, however, we feel that this evident weakness is also a not-so-evident strength: the program runs sufficiently fast that the user is easily able to alter each of the various input parameters over some reasonable range of values and see directly how the astrophysical results are changed when all other inputs are held strictly fixed. We have also explored in detail the behavior of DAOSPEC in several cases of interest, performing a variety of tests that show the range of applicability of DAOSPEC in terms of data quality, and should also help in the search for the best set of configuration parameters for each case. Novice (and experienced!) users are positively encouraged to carry out such experiments. Similarly, feedback from the users is of immense help, allowing us to refine the code in the directions of major interest for the scientific community.

We would like to thank the early testers and users and a few people that gave us useful suggestions and stimulated interesting discussions: Stefano Bagnulo, Katia Biazzo, Giulia Cairra, Eugenio Carretta, Éric Depagne, Patrick François, Raffaele Gratton, Vanessa Hill, Segei A. Levshakov, Livia Origlia, Luca Pasquini, Ignazio Pillitteri, Francesca Primas, Marina Rejkuba, Emanuel Rossetti, Luca Sbordone, Antonio Sollima, Manuela Zoccali. We thank Elizabeth Griffin for a critical reading of the manuscript. We would also like to thank Chris Sneden, Solange Ramírez and Sergio Sousa for providing their codes and their help. We acknowledge the European Southern Observatory in Garching, Germany, where part of this work has been carried out, through the ESO *Studentship* and *Science Visitorship* programmes. E. P. would like to thank the Dominion Astronomical Observatory in Victoria, Canada, for the warm hospitality, and to acknowledge the financial support of the INAF, Osservatorio Astronomico di Bologna, throughout the project.

REFERENCES

- Alves-Brito, A., et al. 2005, *A&A*, 435, 657
- Alves-Brito, A., et al. 2006, *A&A*, 460, 269
- Barbuy, B., et al. 2006, *A&A*, 449, 349
- Barbuy, B., Zoccali, M., Ortolani, S., Minniti, D., Hill, V., Renzini, A., Bica, E., & Gómez, A. 2007, *AJ*, 134, 1613
- Bohlin, R. C., Jenkins, E. B., Spitzer, L., Jr., York, D. G., Hill, J. K., Savage, B. D., & Snow, T. P., Jr. 1983, *ApJS*, 51, 277
- Calabretta, M. R., & Greisen, E. W. 2002, *A&A*, 395, 1077
- Cayrel, R. 1988, *IAU Symp.* 132: The Impact of Very High S/N Spectroscopy on Stellar Physics, 132, 345
- Dall, T. H., Schmidtobreick, L., Santos, N. C., & Israelian, G. 2005a, *A&A*, 438, 317
- Dall, T. H., Bruntt, H., & Strassmeier, K. G. 2005b, *A&A*, 444, 573
- Dall, T. H., Strassmeier, K. G., & Bruntt, H. 2006, *Ap&SS*, 304, 195
- da Silva, L., et al. 2005, *From Lithium to Uranium: Elemental Tracers of Early Cosmic Evolution*, 228, 251
- da Silva, L., et al. 2006, *A&A*, 458, 609
- Edvardsson, B., Andersen, J., Gustafsson, B., Lambert, D. L., Nissen, P. E., & Tomkin, J. 1993, *A&A*, 275, 101
- Fitzpatrick, M. J., & Sneden, C. 1987, *BAAS*, 19, 1129
- Greisen, E. W., & Calabretta, M. R. 2002, *A&A*, 395, 1061
- Greisen, E. W., Calabretta, M. R., Valdes, F. G., & Allen, S. L. 2006, *A&A*, 446, 747
- Jacquinet-Husson, N., Ari, E., Ballard, J., Barbe, A., Bjraker, G. et al. 1999, *JQSRT*, 62, 205
- Jacquinet-Husson, N., Scott, N. A., Garceran, K., Armante, R., Chédin, A. 2005, *JQSRT*, 95, 429

- Kupka, F., Piskunov, N., Ryabchikova, T. A., Stempels, H. C., & Weiss, W. W. 1999, *A&AS*, 138, 119
- Lecureur, A., Hill, V., Zoccali, M., Barbuy, B., Gómez, A., Minniti, D., Ortolani, S., & Renzini, A. 2007, *A&A*, 465, 799
- Letarte, B., Hill, V., Jablonka, P., Tolstoy, E., François, P., & Meylan, G. 2006, *A&A*, 453, 547
- Letarte, B., 2007, Ph.D. Thesis, University of Groningen, The Netherlands
- Levshakov, S. A., Dessauges-Zavadsky, M., D’Odorico, S., & Molaro, P. 2002, *ApJ*, 565, 696
- Meléndez, J., Barbuy, B., Bica, E., Zoccali, M., Ortolani, S., Renzini, A., & Hill, V. 2003, *A&A*, 411, 417
- Monaco, L., Bellazzini, M., Bonifacio, P., Ferraro, F. R., Marconi, G., Pancino, E., Sbordone, L., & Zaggia, S. 2005, *A&A*, 441, 141
- Moore, C. E., Minnaert, M. G. J., & Houtgast, J. 1966, National Bureau of Standards Monograph, Washington: US Government Printing Office (USGPO), 1966,
- Pancino, E., Pasquini, L., Hill, V., Ferraro, F. R., & Bellazzini, M. 2002, *ApJ*, 568, L101
- Pancino, E. 2004, Origin and Evolution of the Elements,
- Pancino, E., Galfo, A., Ferraro, F. R. & Bellazzini, M., 2007, *ApJ*, 661, L155
- Pancino, E. & Stetson, P.B., 2008, *astro-ph/XXXXXXX*
- Pasquini, L., et al. 2002, *The Messenger*, 110, 1
- Pasquini, L., Randich, S., Zoccali, M., Hill, V., Charbonnel, C., & Nordström, B. 2004, *A&A*, 424, 951
- Pence, W. 1999, *ASP Conf. Ser. 172: Astronomical Data Analysis Software and Systems VIII*, 172, 487
- Plez, B., Brett, J. M., & Nordlund, A. 1992, *A&A*, 256, 551
- Pompéia, L., Hill, V., & Spite, M. 2005, *Nuclear Physics A*, 758, 242
- Ramírez, S. V., Cohen, J. G., Buss, J., & Briley, M. M. 2001, *AJ*, 122, 1429
- Rutten, R. J., & van der Zalm, E. B. J. 1984, *A&AS*, 55, 171
- ,Shannon, C. E., 1949, *Proc. Institute of Radio Engineers*, 37, 10
- Shetrone, M., Venn, K. A., Tolstoy, E., Primas, F., Hill, V., & Kaufer, A. 2003, *AJ*, 125, 684
- Snedden, C. 1973, *ApJ*, 184, 839
- Sousa, S. G., Santos, N. C., Israelian, G., Mayor, M., & Monteiro, M. J. P. F. G. 2006, *A&A*, 458, 873
- Sousa, S. G., Santos, N. C., Israelian, G., Mayor, M., & Monteiro, M. J. P. F. G. 2007, *A&A*, 469, 783
- Spite, M. 1967, *Annales d’Astrophysique*, 30, 211
- Stetson, P. B. 1987, *PASP*, 99, 191
- Venn, K. A., & Hill, V. 2005, *From Lithium to Uranium: Elemental Tracers of Early Cosmic Evolution*, 228, 513
- Warmels, R. H. 1992, *ASP Conf. Ser. 25: Astronomical Data Analysis Software and Systems I*, 25, 115
- Wells, D. C., Greisen, E. W., & Harten, R. H. 1981, *A&AS*, 44, 363
- Zoccali, M., et al. 2006, *Revista Mexicana de Astronomia y Astrofisica Conference Series*, 26, 88